SURFACE WETTING METHODS COMPATIBLE WITH SOLID SERS SUBSTRATES

BY

ILYA GOLDSHLAG

THESIS

Submitted in partial fulfillment of the requirements
for the degree of Master of Science in Electrical and Computer Engineering
in the Graduate College of the
University of Illinois at Urbana-Champaign, 2012

Urbana, Illinois

Adviser:

Professor Brian T. Cunningham

ABSTRACT

Nanopatterned metal surfaces are widely used for surface-enhanced Raman spectroscopy. Effectiveness of the sensors depends on how well ligand and analyte molecules can diffuse into the regions of highest enhancement. In liquid phase sensing, this is often contingent upon the ability of the solvent to completely wet the nanostructures.

The topic of surface wetting receives little to no attention in the SERS literature. Yet, wetting experiments on gold SERS nanodomes, used as a case study, resulted in a distinctly hydrophobic behavior, which is incompatible with aqueous sensing. Outside the field of SERS, the effort in surface wetting is usually aimed in the opposite direction, to further reduce surface wetting. Also, the approaches used in those works are typically incompatible with SERS devices.

This document is dedicated to the subject of surface wetting in the context of SERS sensing. Four alternative techniques that can promote complete wetting on nanopatterns without sacrificing SERS efficiency are introduced and discussed in detail. They are: (1) addition of ethanol; (2) addition of surfactants; (3) mild oxygen plasma cleaning; and (4) hydrophilic monolayers. The first two methods modify the solvent, and the last two modify the sensor surface. The general theoretical principles of surface wetting, as well as specific principles for each technique are discussed and complemented by an experimental evaluation of their relative effectiveness in promoting hydrophilicity.

Using some of the developed approaches to aqueous surface wetting, detection of short single-stranded homooligoadenosine in 1 μM solutions is demonstrated for the first time using SERS nanodomes. This is an important milestone on the path to development this substrate into a universal multiplexed sensing platform for disease diagnosis and prevention.

To Julia: my wife, my love, my friend, my support... my everything.

TABLE OF CONTENTS

CHAPTER 1

INTRODUCTION

Nanopatterned metal surfaces are widely used for chemical sensing in solutions by surface-enhanced Raman spectroscopy (SERS). Under proper experimental conditions, monochromatic light of specific frequency illuminating a solid substrate covered with densely packed metal nanoparticles excites localized surface plasmons between adjacent nanoparticles. The intensity of Raman scattering from analyte molecules that happen to be located in the regions of plasmon excitation increases by multiple orders of magnitude, allowing detection of much lower concentrations of analyte within much shorter time and using much less laser power than was previously possible with traditional Raman spectroscopy. However, such enhancement is highly spatially non-uniform and is concentrated almost entirely in the narrowest gaps between adjacent nanoparticles. Hence, the experimentally observed increase in scattering intensity largely depends on how well ligand and analyte molecules can diffuse into the regions of highest enhancement. In liquid phase sensing, this is further contingent on the ability of a solvent to completely wet spaces between nanostructures.

The topic of surface wetting received little attention in the literature devoted to SERS sensing on solid substrates. Since authors do not discuss explicitly the issue of a solvent's influence on wetting, it is unclear whether it factored into the choice of solvent for any given experiment, as did, for example, analyte solubility. Many authors simply assume that the nanostructures on sensor surfaces are fully wetted. In some cases, this assumption happens to be valid. For example, methanol and ethanol used to dissolve common strong Raman scatterers Rhodamine 6G (R6G) and BPE (1,2-bis(4-pyridyl)ethylene) in many proof-of-concept SERS experiments have low enough surface tension to completely wet gold and silver nanopatterned SERS surfaces.

The assumption of complete wetting fails when water is used as a solvent. As will be reported in later chapters, neat water cannot wet sub-50 nm-

wide grooves between SERS nanodomes, which are characteristic of SERS substrates. Instead, water drops retain truncated spherical shapes with contact angles in excess of 120°, which are clearly consistent with non-wetting behavior. Achieving complete wetting with water is extremely important, because water is the solvent of choice in many chemical and biological experiments that are more complex and relevant than mere demonstration of sensor functionality. While some amount of alcohol may be tolerated in many cases, complexity of protocols often precludes a significant replacement of water with an alcohol to achieve better wetting, because the latter may deleteriously interact with other components of the system or degrade the analyte in some way. For example, concentrated ethanol cannot be used in experiments that detect biomarkers excreted by living cells, because in significant concentrations it is deadly for many cell lines. Concentrated alcohols are also incompatible with experiments involving DNA molecules, because they induce conformational changes in DNA and precipitate DNA in the presence of salts.

Outside of the field of surface-enhanced Raman spectroscopy, there exists a large body of literature dealing with wetting properties of patterned surfaces. The main theme of these works is to understand the conditions leading to transitions between non-wetting and wetting behaviors and to enhance hydro**phobicity** for such applications as self-cleaning and microfluidics [1]. The traditional approach to achieving the desired degree of wetting is by optimizing the shape of surface patterns. This approach has extremely limited utility in SERS, where the surface patterns are already optimized for desired optical properties. Besides, the same geometrical attributes that make a good SERS substrate, such as high aspect ratios, dense packing, and tiny gaps between adjacent nanoparticles, also make it less wettable.

In order to improve surface wetting without sacrificing SERS efficiency, it is helpful to consider what properties affect each phenomenon and to identify those unique to each one. SERS enhancement places stringent requirements upon surface geometry, as was mentioned previously. It also necessitates the use of a material capable of sustaining strong localized surface plasmons in the visible spectrum, effectively limiting the choice of surface material to either silver or gold. Spectral location of plasmon resonance depends on the refractive index of the material, which is a bulk material property.

The wetting state is determined by the total surface energy of the solid-liquid system, which, in turn, depends on the interfacial and free surface

energies of the sensor surface and a solvent, as well as on their surface areas. Surface geometry plays an important role in wetting, because it increases the effective surface area of the sensor and makes some regions of the solid less accessible for the solvent. One consequence of dense patterning, for example, is that it further reduces wetting of already poorly wettable surfaces. The outermost layers of interacting media determine their free and interfacial surface energies. The relevant material property is the strength of cleaved intermolecular bonds exposed on the surface of the sensor: stronger bonds result in a stronger tendency to form interfaces by bonding with liquids. Unlike SERS, wetting is sensitive only to the material properties of the outermost molecular layer of the surface; the bulk of non-porous non-absorbent SERS sensors, which are the subject of this thesis, hardly plays a role. Finally, wetting behavior differs dramatically with the choice of solvent, whose surface tension is inversely related to wetting.

The outermost monolayer of the solid and the surface tension of the solvent can both be modified to promote surface wetting of existing SERS sensors without sacrificing SERS enhancement. This thesis investigates and compares four wetting techniques that are based on these two approaches. Two of them modify sensor surface by an oxygen plasma treatment or by a formation of a hydrophilic monolayer. The others reduce the surface tension of the solvent, deionized (DI) water, by an addition of either a miscible (ethanol) or an immiscible (a surfactant) liquid with lower surface tension. In all cases, the effect of varying experimental parameters on surface wetting is reported using the corresponding contact angles. Using an improved wetting protocol, label-free detection of 1 μM thiolated homooligoadenosine on SERS nanodomes is demonstrated for the first time.

Surface wetting considerations raised herein go far beyond the particular SERS sensor technology described herein. They are applicable to any sensor surface used for liquid phase experiments that is either roughened or densely patterned. While the reported contact angle (CA) values are specific to gold nanodomes, the discussed general wetting trends are substrate-independent. Although all of the techniques reported herein are capable of individually inducing a wetting state transition, each one has its unique drawbacks which can render it completely or partially incompatible with particular experimental conditions. It is hoped, however, that the range of discussed techniques is sufficiently diverse, so that at least one approach or,

possibly, a judicious combination of them would be applicable to most sets of experimental conditions.

CHAPTER 2

BACKGROUND

2.1 Surface-Enhanced Raman Spectroscopy

Surface plasmons are collective oscillations of conduction band electrons along an interface between two media, such as a metal and a dielectric, characterized by the opposite signs of the real parts of their dielectric constants. Surface plasmons are generated in response to electromagnetic excitation, when the energy coupling condition is met, that is, when tangential components of the propagation constants of the excitation wave and the surface plasma wave (SPW) match [2]. Surface plasmon resonance manifests as a peak in the extinction spectrum at the resonance wavelength. The propagation constant of a SPW propagating along an infinite planar metal-dielectric interface is given by the following expression:

$$\beta = k_0 n_d \sqrt{\frac{\varepsilon_m}{(\varepsilon_{m,Re} + n_d^2) + j\varepsilon_{m,Im}}} \tag{2.1}$$

where n_d and $\varepsilon_m = \varepsilon_{m,Re} + j\varepsilon_{m,Im}$ are the dielectric constants of the dielectric and the metal, respectively, and k_0 is the propagation constant in free space. As long as $\varepsilon_{m,Re} < -n_d^2$, the resonance condition can be fulfilled. Resonances of several metals, particularly gold and silver, lie in the visible or near-IR region, making them excellent choices for biosensor design.

Because of high loss inside the metal layer, the electromagnetic field of a surface plasmon wave is highly asymmetric. For instance, in the red-to-near-infrared range, 90-95% of the field lies inside the dielectric [2], contributing to high sensitivity of SPR biosensors. The disruption of the resonance condition by the analyte results in a significant increase in reflectance at the resonant wavelength. Three ways to quantify this change – by measuring the changes in peak position [3, 4], resonant wavelength [5, 6], or coupling angle [7, 8] –

have been developed into separate sensing modalities.

SPR biosensors have been extensively used in pharmaceutical research and in many biological experiments, including studies of protein-protein and protein-DNA interactions [9], protein-antibody binding kinetics [10], and biochemical properties of tumor suppressor proteins [11]. Still, SPR biosensors possess a number of significant shortcomings, including inherent lack of analyte selectivity, analyte-ligand size ratio limitations, poor spatial resolution and incompatibility with highly multiplexed system design.

With the exception of a few practical benefits for biosensor design, **localized surface plasmon resonance (LSPR)** spectroscopy is very similar to SPR spectroscopy. Both techniques are capable of real-time kinetic high-sensitivity measurements of changes in the local dielectric environment. Although SPR fields extend 40-50 times farther away from the metal-dielectric interface, making SPR spectroscopy much more sensitive to bulk changes of the refractive index, the smaller detection volume of LSPR makes it better suited for high-resolution measurements.

LSPR is a closely related phenomenon to SPR: it describes energy coupling of electromagnetic excitation fields into collective oscillations of conduction band electrons within small metal nanoparticles surrounded by a dielectric medium. The LSPR dielectric resonance condition can be found using Mie solution that describes electromagnetic fields in a dielectric medium surrounding a single nanoparticle. In case of spherical metal nanoparticles, Mie solution has an analytical form [12]. The maximum of the extinction spectrum depends on dielectric permittivities as follows:

$$E(\lambda) \sim \frac{\varepsilon_{m,Im}(\lambda)}{\left(\varepsilon_{m,Re}(\lambda) + \chi\varepsilon_d\right)^2 + \varepsilon_{m,Im}(\lambda)^2} \tag{2.2}$$

where $\varepsilon_m = \varepsilon_{m,Re} + j\varepsilon_{m,Im}$ and ε_d are dielectric permittivities of the metal and the surrounding dielectric, and χ is a shape factor with a value of 2 for a perfect sphere and larger values for higher aspect ratios. For metals with a negative real part and a small positive imaginary part of the wavelength-dependent dielectric constant, the resonance condition occurs when $\varepsilon_{m,Re}(\lambda) \approx -\chi\varepsilon_d$.

Size, spacing and shape of nanoparticles also influence the location and strength of LSP resonance. The ability to fabricate a broad array of particles using electron beam lithography and chemical synthesis of colloidal solutions has been instrumental in advancing the fundamental understanding of these

dependences. Resulting nanoparticles exhibit tunable resonances throughout the visible and near-infrared regions, which is another major advantage of LSPR in optical sensor design.

Raman spectroscopy is a very promising approach to biosensing with a potential to address most weaknesses of SPR spectroscopy. It is a spectroscopic technique for analysis of low-frequency vibrational modes in molecules using inelastically scattered monochromatic light. In addition to detecting the presence of analyte, it offers detailed information about analyte's molecular structure, because Raman spectra are as unique as the analyte's chemical makeup. However, extreme weakness of scattered light has haunted Raman spectroscopy for many decades: on average, only one in 107 incident photons undergoes Raman scattering. For this reason, the technique remained of little practical interest until the mid-1970s, when a way to greatly enhance Raman scattering cross sections was discovered [13, 14].

Surface-enhanced Raman scattering (SERS, also stands for SER spectroscopy) is a phenomenon, whereby molecular radiative Raman cross sections are greatly amplified by elevated electromagnetic fields of localized surface plasmons (LSP) on metal nanostructures. A medium sustaining plasmons is called a *SERS substrate* regardless of its physical state, solid or liquid. The ratio by which a SERS substrate increases Raman scattering is called the *enhancement factor (EF)*. It is the main quantitative metric for comparing the limits of detection of different substrates. It has two major independent multiplicative contributors: the *electromagnetic enhancement (EME)* [14] and the *chemical enhancement (CE)* [13].

The nature and even the mere existence of the CE effect is subject to debate to this day. Those researchers that do observe CE ascribe it to coupling of electronic states between adsorbed molecules and the metal surface [15]. On the opposite side of the argument, there are some convincing reports that find minimal to no evidence for CE effect [16]. In any case, CE is relatively weak, contributing single- to double-digit enhancements to the overall enhancement factor [17].

EME effect is the strongest contributor to SERS enhancement, responsible for increase of scattering cross sections by a factor of $10^6 - 10^8$ or, under most optimized conditions, by as much as $10^{11} - 10^{12}$ [16, 18]. EME is caused by the excitation of LSPR on closely spaced metal nanoparticles. In the *hot spots*, the regions of highest field enhancement, incident fields are amplified

by tens or hundreds of times. Raman scattering cross section is proportional to the square of the induced dipole moment, which, in turn, is proportional to the magnitude of the incident EM field [19]. Consequently, EME scales with the fourth power of field intensity because the electric fields are enhanced twice, in a multiplicative fashion. First, the analyte in hot spots is subjected to the fields locally enhanced by localized surface plasmons. Then, by a very similar mechanism, Raman-scattered light couples back into LSPs, resulting in the second enhancement, albeit at a different frequency. The resulting EM enhancement factor can be found from the following formula:

$$EF = EF_{ex} * EF_{scat} = \left| \frac{E(\omega_{ex})}{E_0(\omega_{ex})} \right|^2 \left| \frac{E(\omega_{scat})}{E_0(\omega_{scat})} \right|^2 \tag{2.3}$$

where $E_0(\omega_{ex})$ is the amplitude of the excitation field, $E(\omega_{ex})$ is the amplitude of the local electric field in the hot spot after the first enhancement, and $E_0(\omega_{scat})$ and $E(\omega_{scat})$ are, respectively, the initial and enhanced amplitudes of a Raman mode. EF_{ex} and EF_{scat} are the enhancement factors at the excitation and Raman mode frequencies.

This work uses and improves upon nanodomes SERS substrates originally developed in our group by Dr. Charles Choi [20]. The active surface is composed of tightly packed square arrays of gold nanodomes with the center-to-center spacing of 400 nm and the hot spot width of 20-30 nm. This SERS substrate is designed to deliver a uniform enhancement factor across large surface areas. It can be cheaply and uniformly fabricated on plastic film with a roll-to-roll transfer process by nanoreplica molding and with e-beam evaporation, as described in Section 3.1.

2.2 Surface Wetting

Liquid is a state of matter characterized by nearly constant density, but no definite shape. On a macroscopic scale, a liquid assumes the shape of its container, bending and bulging to fill in the crevices. However, any liquid surface has a limited amount of flexibility, which becomes increasingly evident from its interactions with ever smaller grains and textures of a solid. If surface features become sufficiently small and dense, the liquid loses ability to exactly conform to their shape. Instead, it spans over them in relatively smooth

arches, still resembling the general shape of the solid surface, but maintaining only a partial contact with it. The side walls of adjacent microscopic features and the valleys between them remain dry.

In the context of this work, **wetting** is defined as an ability of a liquid to maintain contact with a solid surface. The degree of wetting refers to how well the liquid can permeate surface roughness of given characteristic dimensions, such as nanopatterned indentations and protrusions. It is determined by the opposing action of adhesive and cohesive molecular forces. **Adhesive forces** are responsible for a tendency of two dissimilar materials to bond to each other chemically or mechanically. They increase interface area, promote wetting of surface features, and cause liquids to spread thinly over solid surfaces. **Cohesive forces**, on the other hand, describe a tendency of molecules within a single medium to cling together. In liquids, cohesive forces pull surface molecules into the bulk, giving drops spherical shapes, reduce the surface area of liquids, and minimize contact area with solid surfaces.

Surface wetting can be improved by maximizing adhesion with the solid, while reducing cohesion within the liquid. Achieving complete wetting is an important consideration for SERS experiments performed on solid nanopatterned SERS substrates. Most signal enhancement occurs in the narrowest gaps between adjacent nanofeatures, and the effectiveness of a SERS substrate depends on how densely ligands and analytes can populate them.

Surface wetting is commonly studied by analyzing behavior of a drop placed on a solid surface of interest. The degree of surface wetting and the equilibrium shape of the drop can be understood from the tendency of all physical systems to minimize their potential energy. **Surface energy** is a type of potential energy defined as the amount of work required to create a unit of surface area from the bulk of a given material. It is denoted by γ and is equal to half the work (W) of cleavage: $\gamma = \frac{1}{2}W$. The factor of one half comes from the fact that a single cleavage creates two new surfaces. Surface creation is an endergonic process, where the energy is expended on breaking chemical bonds between molecules of newly formed surfaces. Molecules comprising the surface of a liquid or a solid, therefore, have elevated potential energies relative to the molecules of the bulk. Therefore, any rearrangements within a solid-liquid physical system that lead to reduced surface energy are energetically favorable.

Surface energy of a solid can be lowered by wetting. The energy of molecules comprising the surface is reduced by replacing cleaved bonds with chemical

(ionic or covalent) or physical (dipole-dipole) bonds with the liquid. The resulting potential energy per unit area is called the **interfacial surface energy** and denoted by γ_{SL}. This value depends on both the strength and the density of interfacial bonds, which vary based on chemical composition of both materials.

The total surface energy of a system comprised of a drop sitting on a solid surface of area AS is the sum of all surface and interfacial energies:

$$E = E_{LG} + E_{LS} + E_{SG} = A_{LG}\gamma_{LG} + A_{LS}\gamma_{SL} + (A_S - A_{LS})\,\gamma_{SG} \tag{2.4}$$

where the subscript LG refers to the drop's dome-shaped free surface, LS – the contact area between the two media, SG – the free solid surface, and E, A and γ represent interfacial or free surface energy, surface area, and interfacial or free surface tension, respectively.

An incremental advance or recession of the wetting front takes place, so long as it is accompanied by a reduction in the total potential energy:

$$\frac{dE}{dA_{LS}} = \frac{dA_{LG}}{dA_{LS}} * \gamma_{LG} + \gamma_{SL} - \gamma_{SG} < 0 \tag{2.5}$$

A stable equilibrium shape of a drop corresponds to a local minimum in the potential energy:

$$\frac{dE}{da} = 0 \tag{2.6}$$

and typically resembles a truncated sphere.

Experimentally, the degree of wetting can be conveniently estimated from the **contact angle**: the angle formed by the plane of the solid and the tangent to the drop's surface, taken at its base.

When a drop surrounded by gas rests in equilibrium on a flat rigid surface, the net force acting on the boundary between the three phases must be zero. In the case of an ideally smooth, rigid, insoluble and homogeneous surface, the three relevant forces are those associated with the surface tensions of the liquid (γ_{LG}) and solid (γ_{SG}) and the interfacial surface tension (γ_{SL}), as shown on Figure 2.1. The relation between them is described by the Young's equation:

$$\gamma_{SG} = \gamma_{SL} + \gamma_{LG}\cos(\theta) \tag{2.7}$$

where θ is the contact angle.

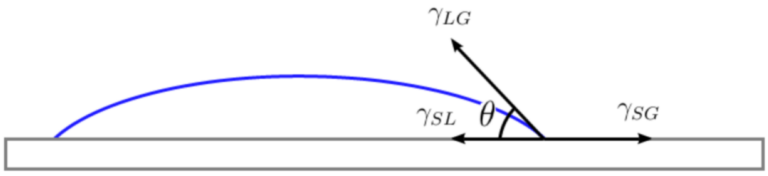

Figure 2.1: Forces associated with the free surface tensions of liquid (γ_{LG}) and solid (γ_{SG}) and the solid-liquid interfacial surface tension (γ_{SL}) acting on a liquid front of a drop placed on an ideal flat surface. The angle between the solid-liquid interface and the slope to the drop's curved surface is called the contact angle. When a drop is in equilibrium, the net force acting on the liquid front must be zero.

Solids whose surface energy is reduced by interfacing with a liquid ($\gamma_{SL} < \gamma_{SG}$) are called wettable by that liquid. In the equilibrium state of a drop resting on a flat rigid solid, the horizontal projection of the force of liquid's free surface tension must point toward the center of the drop, balancing the force of free surface tension of the solid that pulls the liquid front outward. Drops in equilibrium spread broadly on such surfaces, exhibiting values of contact angles below 90°. Then the liquid is water-based, such surfaces are called hydrophilic; otherwise, the term lyophilic is used.

Conversely, on poorly wettable surfaces, the contracting force of interfacial tension is larger than the spreading force of the free surface energy of the solid. In equilibrium, the force of liquid's free surface tension must point away from the center of the drop, resulting in contact angles larger than 90°. Surfaces of this type are called hydrophobic or lyophobic, depending on the liquid. Under critical conditions, when $\gamma_{SG} > \gamma_{SL} + \gamma_{LG}$, Young's equation has no solution for the contact angle. The drop is incapable of maintaining a circular liquid front and spreads uncontrollably over the surface as a thin film.

Wetting analysis of SERS nanodomes substrates, just like that of any roughened surfaces, builds on the same principles as the analysis of flat surfaces. The equilibrium shape of a drop is still characterized by the minimum of total surface energy; however, there are three possible wetting states.

If the solid-liquid interface is composed of dry patches formed by trapped air pockets and of wet patches, where the nanodomes and liquid touch, the

wetting is heterogeneous and described by the Cassie-Baxter model [21]. Liquid interface spans across air gaps between adjacent features without wetting side walls or the valleys between them. Alternatively, if the grooves between nanodomes underneath the drop are completely filled with liquid, the surface is said to be homogeneously wetted. This state is described by the Wenzel model [22]. This is also a non-wetting state, although to a lesser degree. It is characterized by a complete wetting of surface texture underneath the drop. Finally, if the surface is in the hydrophilic, or wettable, state, the drop is unable to maintain a rounded shape and spreads uncontrollably into film across the surface.

The wetting state for a given combination of a solid and a liquid is experimentally determined from the contact angle measurements. Angles in excess of 90° are typically associated with the Cassie state, while the Wenzel state corresponds to contact angles below $\frac{\pi}{2}$. When the contact angle falls below a certain value known as the critical contact angle ($\theta_c \leq \theta \leq \frac{\pi}{2}$), which depends on surface roughness and the fraction of the solid-liquid interface that is wetted [23], a transition to the complete wetting state occurs.

In this document, four methods to promote surface wetting of SERS nanodomes are evaluated. Two methods improve surface wetting by reducing surface tension of the liquid (water), either by addition of ethanol or a surfactant. The other two reduce surface tension of the solid by an oxygen plasma treatment or by forming a hydrophilic monolayer on the nanodomes. In all cases, contact angle measurements are used to optimize the experimental parameters to achieve a transition to the Wenzel state.

CHAPTER 3

INSTRUMENTS, MATERIALS AND METHODS

3.1 Substrate Fabrication

Nanodomes arrays were fabricated on flexible plastic sheets by replica molding and electron beam evaporation. A detailed summary of the fabrication procedure is provided next, with additional details found in the literature [20].

A master mold for replica molding was fabricated on the surface of an 8 inch silicon wafer by step-and-repeat nanoimprint patterning process, using an 8 x 8 mm^2 dye over 120 x 120 mm^2 area. The wafer was patterned with a two-dimensional square array of cylindrical holes with 300 nm diameter, 130 nm depth, and 400 nm pitch and etched using reactive ion etching. The cleaned silicon mold was immersed into dimethyldichlorosilane for 5 minutes and rinsed with ethanol and water. The silane creates a hydrophobic layer on the master mold surface, which promotes a clean release of cured polymer replicas during nanodome fabrication.

The fabrication procedure for a nanodomes substrate is schematically illustrated on Figure 3.1. Twenty drops of a liquid UV-curable acrylate-modified silicone polymer Zipcone UA (Gelest) were pipetted onto the silicon master mold. A 250 μm-thick sheet of clear polyethylene terephthalate (PET) was slowly applied over the liquid polymer from one end with a heavy Teflon roller, spreading the polymer uniformly between the master mold and the PET sheet.

The polymer was cured by slowly translating it on a motorized stage under a Xenon lamp twice over a period of 90 seconds. The Xenon lamp with a pulse rate of 120 Hz and pulse duration of 25 μs had nearly flat emission intensity of 50 mW/cm^2 in the spectral region of sensitivity of the polymer (240-365 nm). Once cured, the PET substrate was peeled away from the

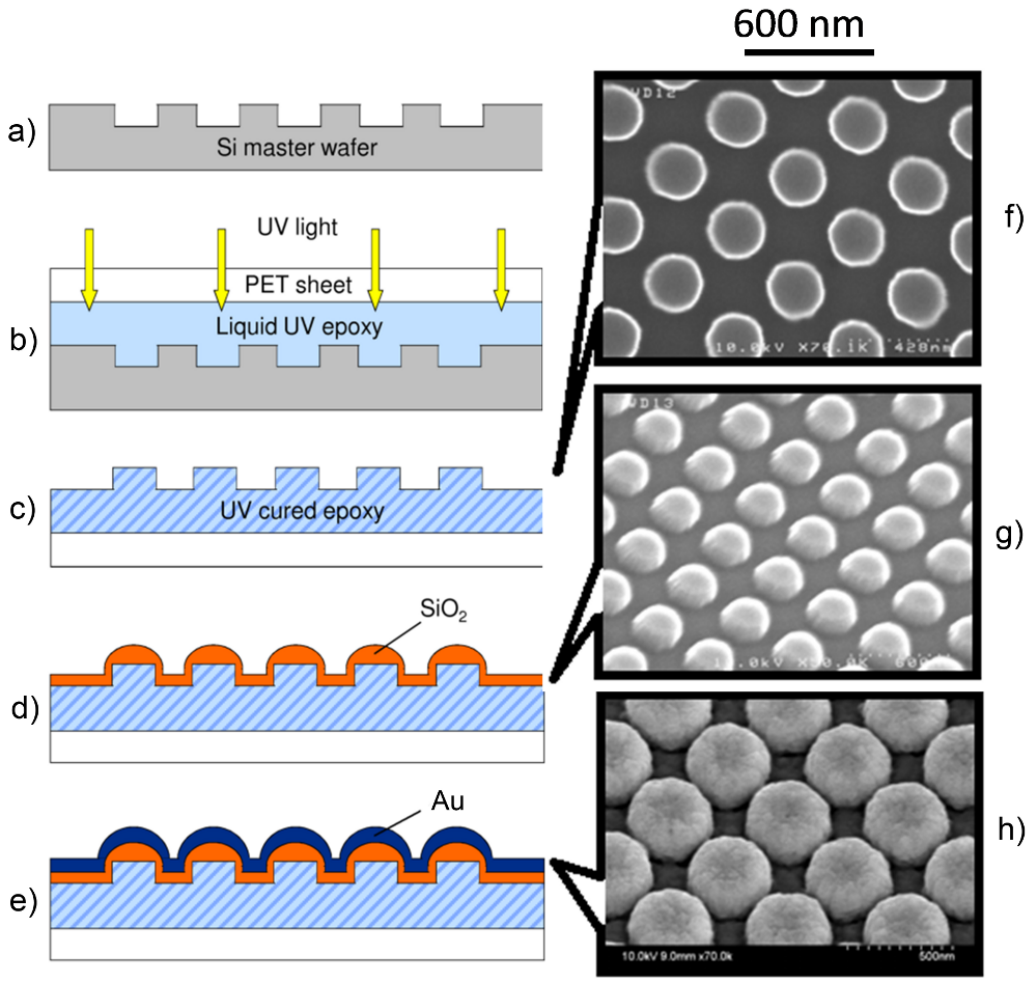

Figure 3.1: Schematics of the fabrication process of gold SERS nanodomes. (a) Silicon master mold covered with a rectangular array of cylindrical holes 300 nm in diameter and 400 nm apart. (b) Regular cylindrical pillars are molded into a liquid UV-curable polymer and solidified with UV light. (c) Released nanopillar arrays adhered on a flexible PET sheet. (d) E-beam evaporated spacer layer of SiO_2 with thickness of 70 nm. (e) Final fabricated nanodome structures after e-beam evaporation of a 130 nm layer of gold. (f) SEM top view image of structures in figure (c). (g)-(h) SEM side views of structures in figures (d)-(e), tilted by 30° from the normal.

master, releasing arrays of cylindrical pillars (Figure 3.1c).

Following replica molding, the nanopillar surface was coated with a 70 nm layer of SiO_2 in an electron-beam evaporator (Denton Infinity 22), to control the spacing between the side walls of adjacent nanodomes, which is an important parameter for SERS enhancement. Finally, a Temescal electron beam evaporator was used to coat the nanodomes with a 10 nm adhesion layer of titanium and a 130 nm layer of gold, creating a medium capable of supporting localized surface plasmons that produce the desired field enhancement. The SEM images of completed devices are shown on Figure 3.1h. Fabricated substrates were stored in a vacuum-assisted desiccator until use.

3.2 Instrumentation

3.2.1 Goniometer

KSV Instruments' Contact Angle Meter (CAM), hereafter referred to as the goniometer, was used to measure all contact angles reported in this work. All contact angle measurements were performed in a class 100 cleanroom facility.

A stock photograph of the goniometer is shown on Figure 3.2. The goniometer was equipped with an automatic liquid dispenser with disposable tips mounted on a motorized vertical translation stage, which deposited drops of precisely controlled volume on gold surfaces. The interface unit on the left-hand side of the instrument housed the electronics and a monochromatic blue LED light source mounted in a reflective sphere. The LED illuminated the drop from behind. Monochromatic light assured a sharp image free of chromatic aberrations and minimized sample heating that may have led to inaccurate measurements due to evaporation.

A tip/tilt adjustable sample stage positioned the sample in front of the light source and underneath the liquid dispenser and aligned it horizontally. It was mounted on an adjustable-height post attached to a two-dimensional XY translation stage with manual micrometer leadscrews. That entire stage assembly moved along the central rail between the light source and the camera that allowed coarse position adjustment.

A 30 fps FireWire camera with 512 x 480 resolution sent a live video feed to a computer for measuring drop size and the contact angle with the sample.

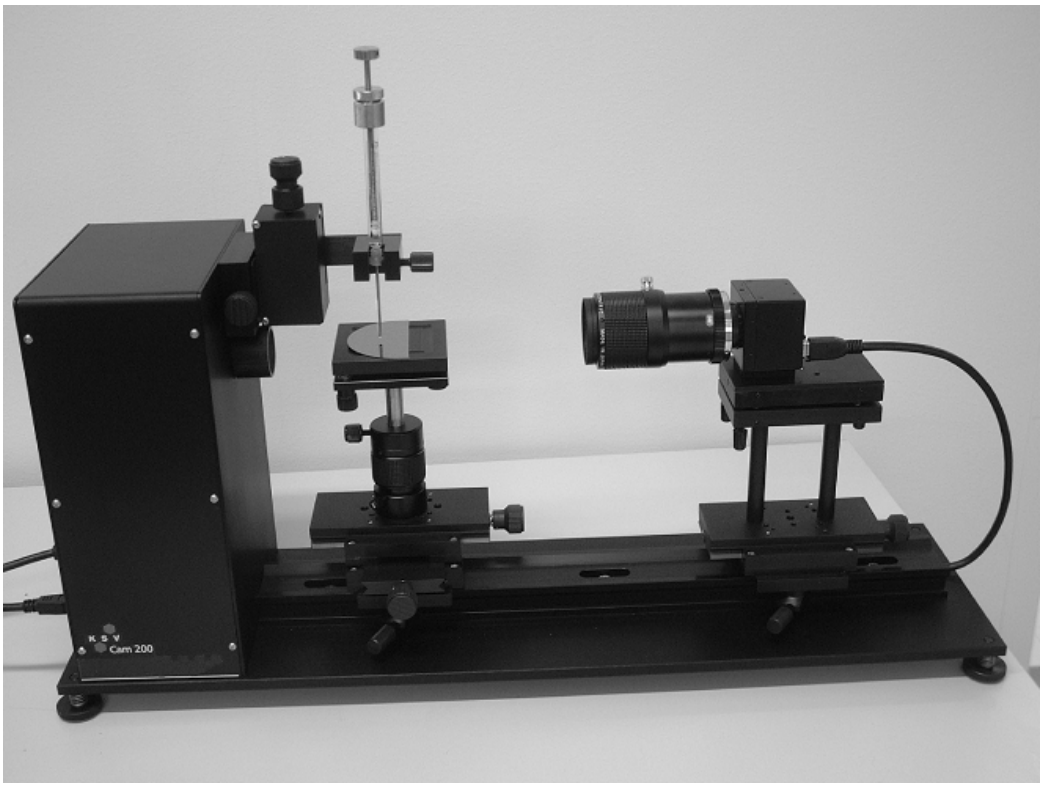

Figure 3.2: A stock image of KSV Instruments' CAM 200 goniometer used to measure contact angles. An automated dispenser places drops onto leveled substrates. The drops are photographed by a digital camera shown on the right, and the software automatically measures the drop's dimensions, volume, contact area and contact angles.

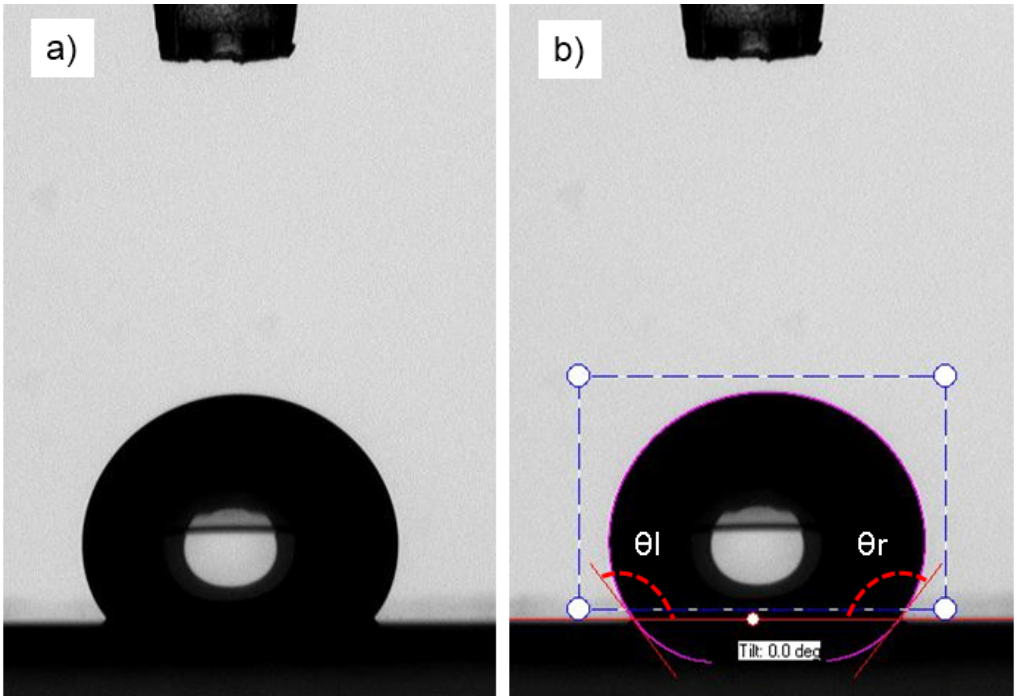

Figure 3.3: (a) A raw image of a 6 μL drop of neat DI water dispensed onto an untreated gold nanodomes substrate. (b) The same drop after being processed by the software. The shape of the drop is approximated, from which all relevant metrics including the contact angles are calculated.

Multiple measurements could be taken at specified time intervals to observe kinetic behavior of the drop.

A typical raw image obtained from a goniometer is shown on Figure 3.3a, from which the computer approximated the shape of a drop and computed left and right contact angles, width, height, volume and the contact area of a drop. A processed image of the same drop is shown on Figure 3.3b.

3.2.2 Oxygen Plasma Etcher

March Jupiter III reactive ion etcher located in the same cleanroom as the goniometer was used to evaluate the ability of oxygen plasma treatment to improve surface wetting. A photograph of the actual system used is shown on Figure 3.4. It is a parallel plate reactive ion etcher with a 13.56 MHz fixed frequency RF generator and a 300 W maximum power output. The top-loading chamber is large enough to accept 4 inch wafers. The chamber electrodes are designed to maximize anisotropy and uniformity of an etch. Both electrodes had water cooling to maintain the chamber at a low temperature during processing.

3.2.3 Raman Microscope

Surface-enhanced Raman spectroscopy on SERS nanodomes was performed using a Renishaw mircoPL / inVia Raman microscope, such as one shown on Figure 3.5. All measurements were taken in a darkroom.

An inVia microscope is a versatile Raman/SERS system with multiple interchangeable components and modules. The configuration used for this work utilized a 100 mW 785 nm diode laser attenuated with neutral density (ND) filters to deliver 1.1 mW of power to the sample plane. The excitation light was focused on a sample through a 20x objective of a Leica DM2500M microscope with NA = 0.4. A motorized translation stage positioned the sample under the objective with 2 um precision in the transverse XY plane. Focusing in the Z direction was performed by manual coarse leadscrews of the Leica microscope and by a high-precision automated piezoactuated vertical translation stage with sub-100 nm precision.

The collection path was equipped with a video camera that sent a live feed

Figure 3.4: March Jupiter III RIE used to treat SERS nanodomes with oxygen plasma. The sample chamber is on top of the main module on the upper shelf, which also controls vacuum pumps and gas flows. The lower unit is the power supply for the plasma generator.

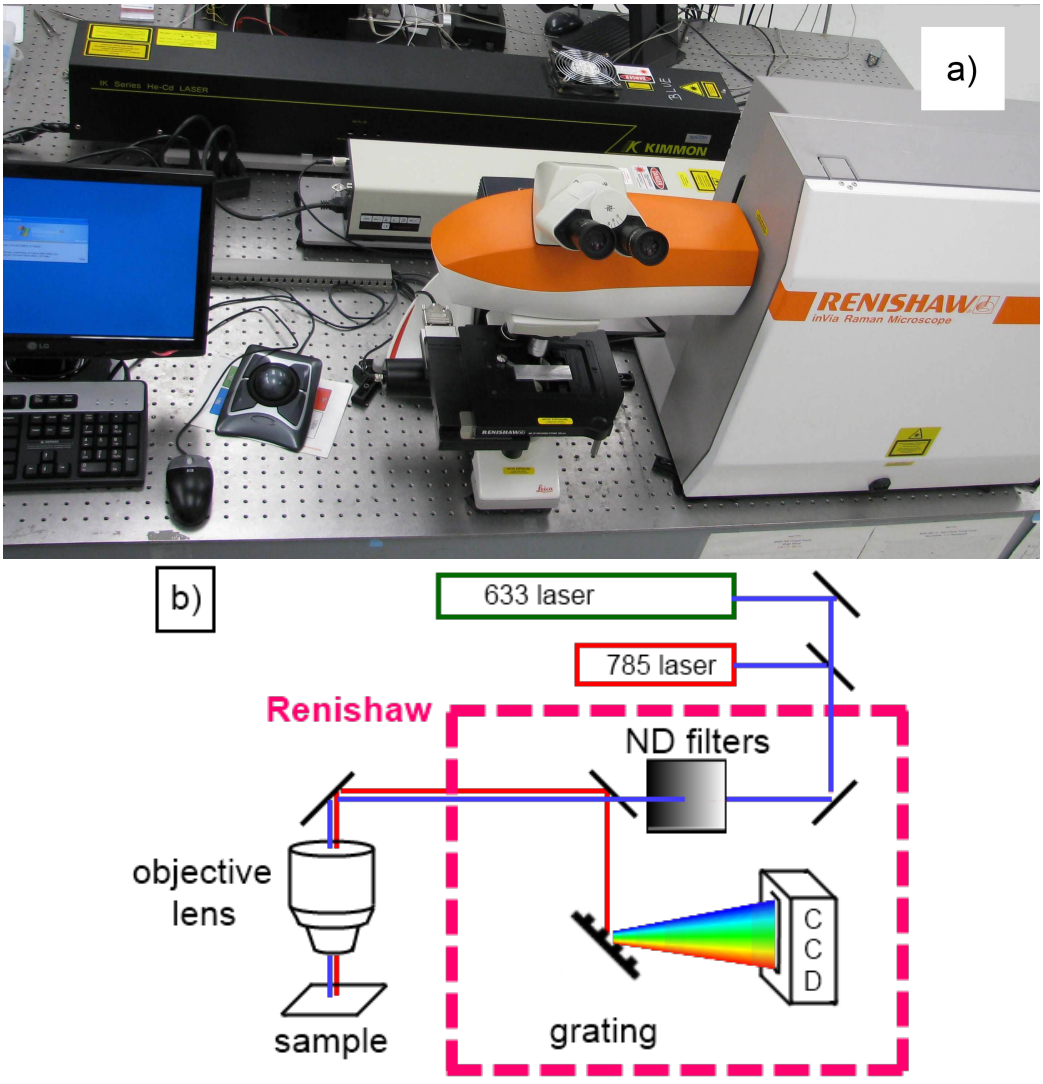

Figure 3.5: (a) The Renishaw inVia Raman/SERS microscope used to perform the label-free homooligoadenosine detection experiments. (b) A simplified schematic diagram of the microscope configuration used to perform the measurements. A 1.1 mW 785 nm excitation laser beam of controllable intensity was focused on a gold SERS nanodomes coupon through a 20x objective with NA = 0.4. The scattered light was dispersed by a 600 l/mm grating and collected with an internal CCD camera.

to the computer monitor to further assist the alignment and focus. Back-scattered Raman light was collected by the same 20x objective, and the excitation line was removed by a 100 cm^{-1} edge filter. Transmitted light passed through a confocal slit and was dispersed by a 600 l/mm diffraction grating onto a 578x400 pixels UV-coated deep depletion CCD array detector sensitive in the range of 200-1050 nm.

3.3 Protocols

3.3.1 Common Procedural Steps for All Wetting Techniques

Unless otherwise stated, every CA measurement was performed on a single drop of solvent deposited on a fresh gold surface. All drops used in this work were 6.0 $\pm$ 0.1 μL. Every drop was photographed 5 times at 1 second intervals, and the contact angle values were averaged. All experiments were performed in duplicates, and the reported CA values are averages. A fresh pipette tip was used for each new liquid. Each contact angle measurement on a nanodomes surface was accompanied by a reference measurement on a flat gold surface under the same experimental conditions.

A single drop was dispensed as follows. First, a desired volume of liquid was ejected, forming a drop suspended from the dispenser pipette tip. The motorized stage was lowered until the drop touched the substrate, resulting in a transfer of the entire ejected volume onto the substrate, and then immediately withdrawn. The contact angle was measured immediately afterward.

Ethanol dilutions were prepared from deionized water ($\Omega \approx 17$ MOhm) and house 100% ethanol further dehydrated with Type 3A molecular sieves (Sigma-Aldrich). All percent concentration values stated in this work are by volume.

3.3.2 Ethanol Concentration Series

The effect of concentration of ethanol on the wetting properties of its aqueous solution was studied by measuring the contact angles of drops of various dilutions on fresh nanodome substrates. A dilutions series with 0%, 12%,

25%, 30%, 33%, 35%, 40% and 66% of ethanol in DI water was prepared and used.

3.3.3 Oxygen Plasma

The March reactive ion etcher was operated in manual mode. The oxygen flow was adjusted to result in process pressure of 0.8 mTorr. The generator output power set to 50 W. The duration of etch between 4 and 75 seconds was specified by a particular experiment. Samples were treated with oxygen plasma one at a time, to minimize delays to measurement. Wetting was analyzed using 20% ethanol solution. All contact angles were measured in the first 10 minutes following the plasma treatment. After the CA measurements, all treated samples were imaged in SEM for any damage resulting from oxygen plasma. None was found.

3.3.4 Hydrophilic Monolayer

A self-assembled hydrophilic monolayer was formed on gold surfaces by incubating a 3 mM aqueous solution of 6-mercaptohexanol (Sigma-Aldrich) for 15 minutes on gold in a covered Petri dish, in a humidity-controlled environment.

After the incubation, excess solution was aspirated, and gold surfaces were rinsed for 30 seconds with ethanol, then for 30 seconds with DI water, and then dried with nitrogen gas. Contact angle measurements were performed on the following day, using 0%, 10%, 20%, 30% and 40% ethanol.

3.3.5 Surfactants

The three surfactants tested in this work were Tween-20, Triton X-100 and SDS. Two dilutions of 0.1% and 0.01% in DI water were prepared from each compound and mixed by vortexing. Contact angles were measured at 15 second intervals for 4 minutes following drop deposition, providing sufficient time for drop spreading and contact angle stabilization.

3.3.6 Oligonucleotide Immobilization

Oligonucleotides were purchased from BioSearch Technologies. Single-stranded homooligoadenosine 26-mers were functionalized with a 5-Thio C6 (thiohexyl) group at the 5' terminus and purified by dual HPLC. A 1 μM oligonucleotide solution was prepared with 10 μM MgCl2 and 0.1% Triton X-100 in TE buffer. Approximately 35 μL of solution was pipetted onto each nanodomes coupon, covering them completely, and incubated in a covered Petri dish under controlled humidity, to minimize evaporation of the solvent. After 2 hours, the remaining solvent was rinsed for 30 seconds with 0.1% aqueous solution of Triton X-100, followed by a 30 second rinse with DI water, and dried with a nitrogen gun.

CHAPTER 4

SURFACE WETTING TECHNIQUES

4.1 Procedural Notes

4.1.1 Reusability of SERS Sensors

It would have been ideal to use a single gold nanodomes coupon to completely characterize surface wetting. This approach would have minimized any variations due to surface defects and non-uniformities. However, both water and diluted ethanol left annular stains on nanodomes visible to the naked eye upon drop removal. The values of contact angles measured on stained substrates differed significantly from analogous measurements on unused substrates. Figure 4.1 shows contact angles for an ethanol concentration series experiment performed entirely on a single reused coupon, as well as the matching data on flat gold. The wetting state transition did not occur near the expected transition point of 30% of ethanol, as evidenced from contact angle values for patterned gold remaining above 80° and from a significant angle difference with the flat gold state.

The stains could not be washed away either by rinsing or by soaking coupons in DI water or ethanol. However, upon baking the sensors for a minimum of 2 hours at 70 °C in a vacuum oven, the stains disappeared. The stains were probably caused by trace amounts of liquid trapped in the grooves of patterned surfaces, and they managed to interfere with consequent experiments. Although some progress was made in removing stains, long baking times made reusing coupons impractical.

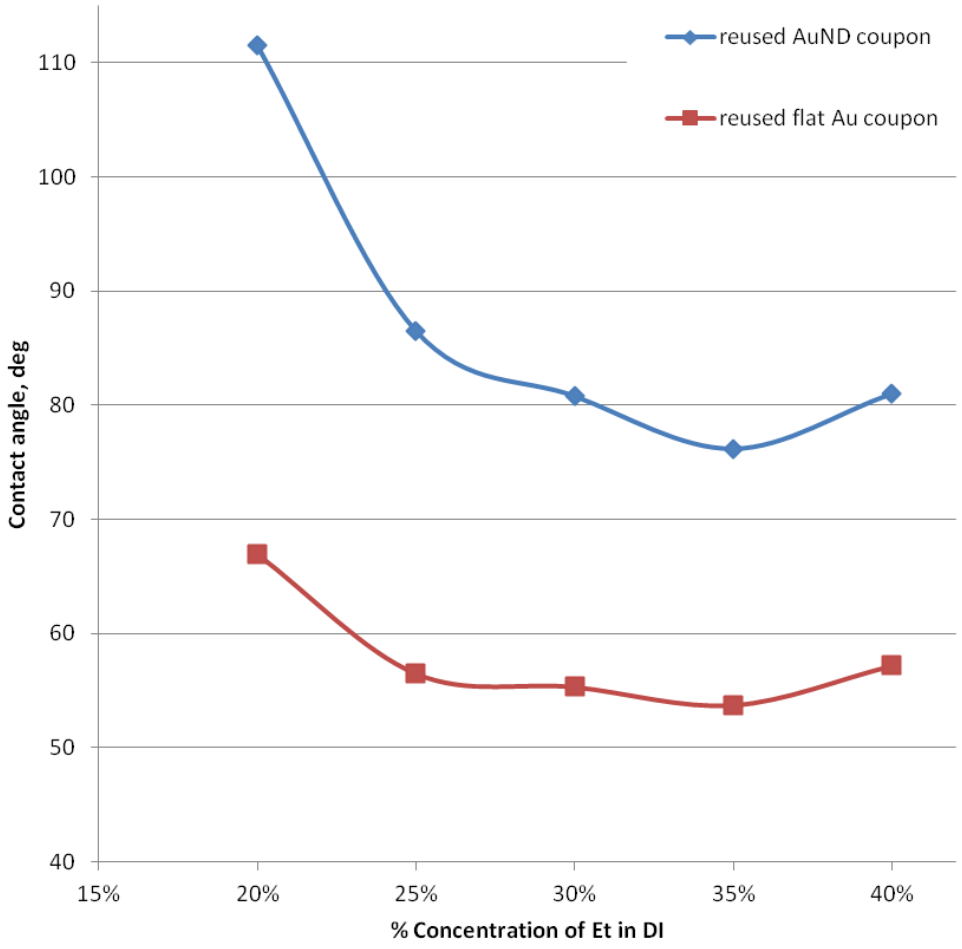

Figure 4.1: Contact angles of a dilution series of ethanol measured on reused flat (red squares) and patterned (blue diamonds) gold surfaces. Surfaces were thoroughly dried for 30 seconds with nitrogen gas before every reuse. Wetting state transition did not occur near a 30% mark, as it did when fresh sensors were used, precluding reuse of test surfaces.

4.1.2 Reproducibility of Measurements

The method that was ultimately used to collect data involved measuring each data point on an unused region of a substrate. In order to assess the reproducibility of acquired data, 8 identical drops of DI water were spotted and measured on two coupons, 4 drops per coupon. The results are shown on Figure 4.2. The contact angles averaged over an entire coupon were found to be 127.1° ± 1.1° and 123.5° ± 2.4°, showing a very good uniformity across a single coupon and between coupons. This finding allowed to conclude that contact angle values measured on different pieces of nanodomes substrate can be compared directly, and that any variation due to substrate non-uniformity or surface defects would be insignificant.

4.2 Dilution of Water with Ethanol

Surface tensions of liquids may differ manyfold. At 20 °C, surface tension of neat water is 72.75 mN/m, which results in a Cassie-Baxter wetting state on a nanodomes surface. By mixing water and liquids with lower surface tensions [24], it is possible to reduce the surface tension of the mixture significantly enough to induce a wetting state transition. Ethanol is a good candidate, because at room temperature its surface tension is only 22 mN/m, and it assumes a lyophilic wetting state on SERS nanodomes. Additionally, ethanol is readily available, non-toxic, dries easily and dissolves many compounds, including some of the most common SERS dyes, such as R6G and BPE.

The limitation of this approach comes from ethanol's incompatibility with some important classes of analytes and experimental conditions. As was discussed in the introduction, concentrated ethanol can denature or precipitate DNA molecules, such as DNA aptamers, and disrupt cell membranes. Whereas dilute ethanol solutions are often tolerable, the destabilizing effects of ethanol on biological molecules or systems increases with concentration.

The goal of this experiment is to understand the influence of the amount of ethanol on the wetting properties of the mixture on nanodomes surfaces, and to achieve the desired wetting by using a minimum amount of ethanol. Figure 4.3 captures the contact angle dependence vs. ethanol concentration for 6 μL drops of 0% to 66% aqueous solutions of ethanol spotted on both flat and nanodome gold surfaces. In the absence of ethanol, the contact angles or

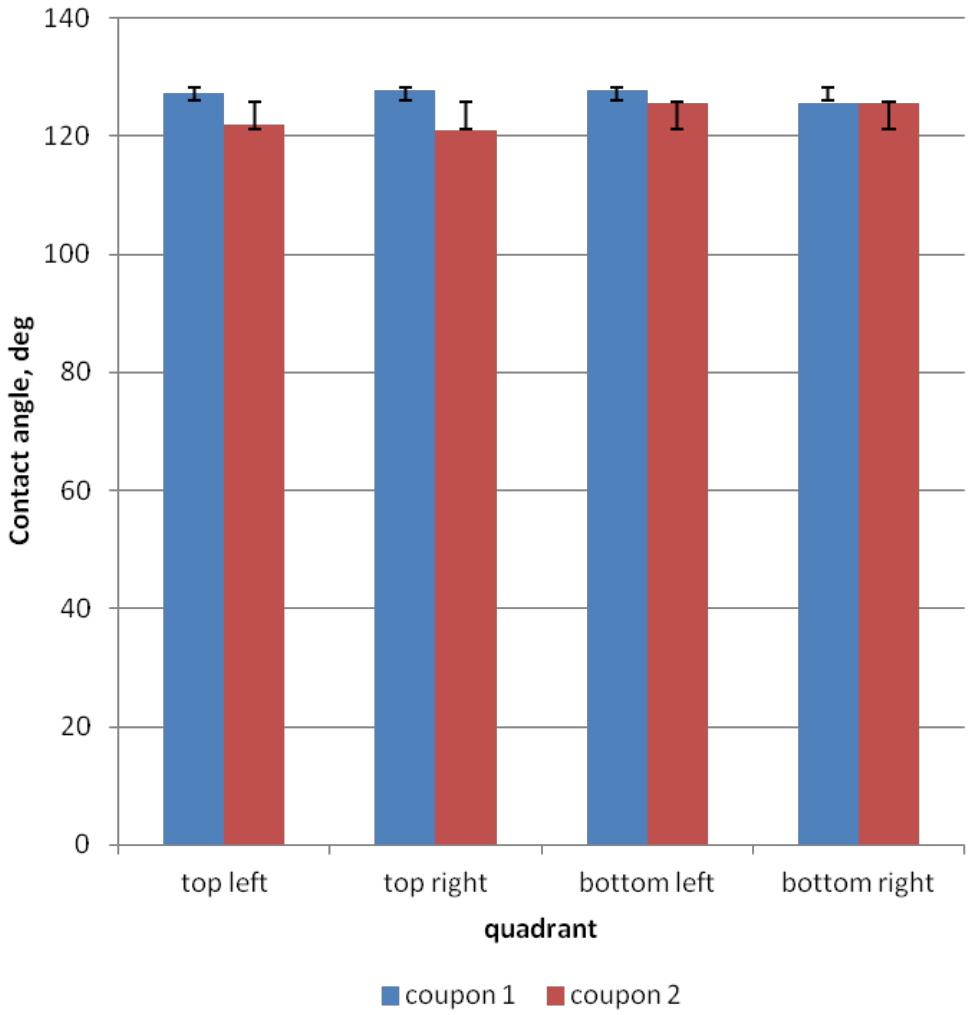

Figure 4.2: Uniformity of contact angle measurement of neat DI water on untreated unused substrate across a single coupon and between coupons. Color bars of the same color represent measurements taken on the same coupon. Standard deviations of 1.1° and 2.4° within each coupon indicate high reproducibility of contact angle values.

pure water were found to be 127° and 85°, respectively. The large difference in contact angle values implies different wetting modes. Since the only difference between the two types of surfaces is their profile, the nanodome surface must be in the non-wetting Cassie state, with air pockets trapped in the gaps between adjacent features.

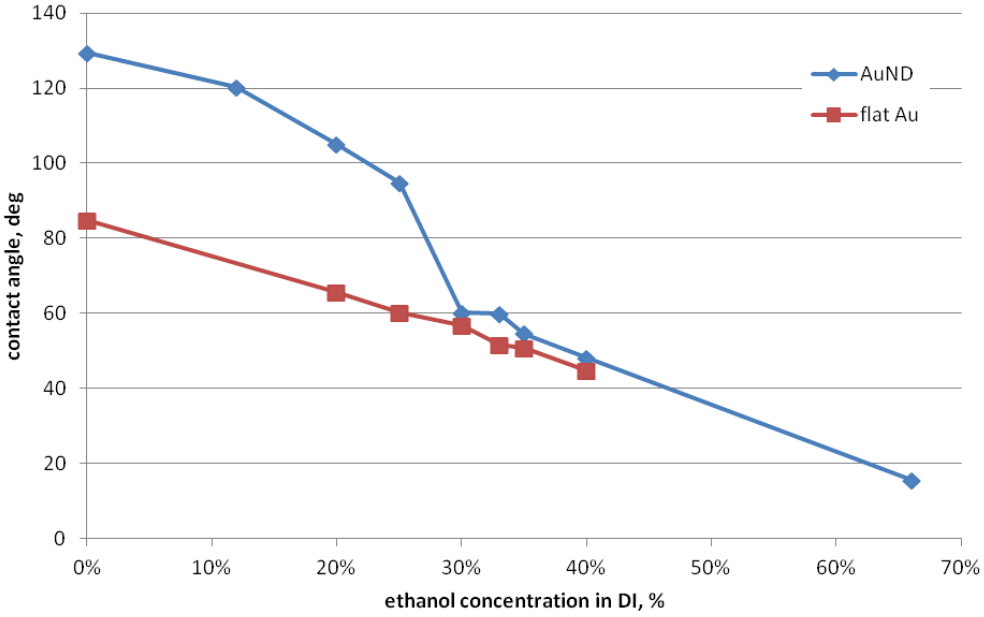

Figure 4.3: Effect of adding ethanol to DI water on the wetting properties of the mixture. Blue diamonds correspond to the contact angles measured on gold nanodomes, and red squares – on flat gold. A wetting state transition takes place on nanodomes near the 30% mark.

As the concentration of ethanol is increased to 30%, the contact angle value drops abruptly, indicating the wetting state transition. Thereafter, the value of CA on nanodomes mimics the flat surface. Therefore, at least a 30% solution of ethanol is required to wet a nanodomes surface. This value is affected by surface geometry, as well as the type of material used, and should be empirically estimated for each type of nanopatterned surface.

A corresponding theoretical value may be derived from the maximum allowed surface tension favoring the Cassie state. However, those calculations typically assume pure surfaces and neglect to take into account the strong hydrophobic effects of surface contaminants introduced during both fabrication and storage. Evidently, even though pure gold is known to be hydrophilic, the contact angle of water on flat gold was nearly 90°.

4.3 Oxygen Plasma Treatment of Substrates

Oxygen plasma treatment subjects material samples to a collection of free radicals, ions and electrons produced from oxygen gas by a high energy radio frequency (RF) power source under the right physical conditions. The surface of the material placed in the chamber is bombarded by very chemically reactive charged particles accelerated by a DC field. The changes induced in the material are complex and depend, among other factors, on gas chemistry, process pressure and sample composition.

Depending on the material treated, oxygen plasma can improve wetting by one or both of the following mechanisms. Firstly, it cleans and etches surfaces, removing surface contaminants, especially organic molecules, that are often more hydrophobic than the bulk material. Surface molecules are broken down by chemical reactions with reactive species in the plasma, and the smaller pieces are volatilized and removed from the chamber by a vacuum pump. Secondly, oxygen plasma may perform surface activation by implanting chemical functional groups onto the surface of a material that increase its surface energy. This improves adhesion and wetting properties of some treated materials.

One of the advantages of oxygen plasma treatment is that only a few outermost atomic layers are affected, while the bulk of the material remains unaltered. Furthermore, plasma does not passivate the nanodomes surface, like monolayer formation does, so it is possible to immobilize molecules on a treated sensor surface. Additionally, it is a directional approach, in which only the top layer of the sensor is attacked, leaving the underlying polymer layers intact.

An important shortcoming of this wetting approach is that it does not have a lasting effect. Although under strictly controlled storage conditions it may be possible to prolong it, the hydrophilicity induced by oxygen plasma usually diminishes between a few hours and a couple of days, so the sensor has to be used promptly. Oxygen plasma cannot be used, once the first layer of organic molecules (e.g. ligands) is applied. It is a violent process that indiscriminately destroys organic molecules.

Even if there are no desirable organic molecules on sensor surface, oxygen plasma should still be used with care on optical sensors. Highly energetic oxygen plasma can damage inorganic nanoscale structures and films, causing

anything from surface roughening to removal and redeposition of device material, and even large-scale film delamination and wrinkling. For example, Figure 4.4 illustrates the damage inflicted to nanodome substrate by exposing it to a plasma treatment under a set of conditions typical for semiconductor microfabrication. Figure 4.4a,b shows the result of a 2-minute-long plasma treatment at the pressure of 0.8 mT and the oxygen plasma generator power P = 100 W. Individual nanodomes were severely roughened and etched back, and became lumpy. Small pieces of surface material were removed and re-deposited in the diamond-shaped gaps between the nanodomes. Not surprisingly, the damaged substrate completely lost its SERS properties. Longer exposure to oxygen plasma led to defects on a larger scale, as shown on Figure 4.4c,d. Multiple wrinkles and fractures formed throughout the metal layer on the scale of 10s to 100s microns and larger; some as large as to be obvious to the naked eye.

Lowering the power level of the oxygen plasma generator may prevent surface damage. In this work, a reduction of generator power to 50 W resulted in no observable damage after a 75-second-long treatment under otherwise the same experimental conditions (see Figure 4.4e,f). Although the associated reduction in the ability of oxygen plasma to remove organic residue is unclear, plasma treatments had a profound effect on improving wetting properties of gold nanodomes.

Figure 4.5 shows the contact angle between the surface of a 6 μL drop of 20% aqueous ethanol and a nanodomes substrate. Apparently, most of the hydrophilic effect is imparted onto the substrate in the first few seconds of treatment. After only 4 seconds of exposure, the nanofeatures were rendered completely wettable, as evidenced from the reduction of the contact angle from 102° to 39°. Longer exposure to oxygen plasma had marginal effect. No significant difference was observed between 30, 45 or 60 seconds of exposure: the contact angle value was nearly constant at 27°. After 75 seconds of exposure, the drop could no longer maintain its rounded shape. Upon deposition, it spread non-uniformly in all directions, making contact angle measurements impossible.

A cumulative effect of multiple wetting approaches is demonstrated on Figure 4.6. Aqueous solutions containing 0, 10 and 20% of ethanol were compared under equivalent conditions on nanodome substrates treated for 60 seconds by oxygen plasma. Addition of alcohol to DI water further reduced

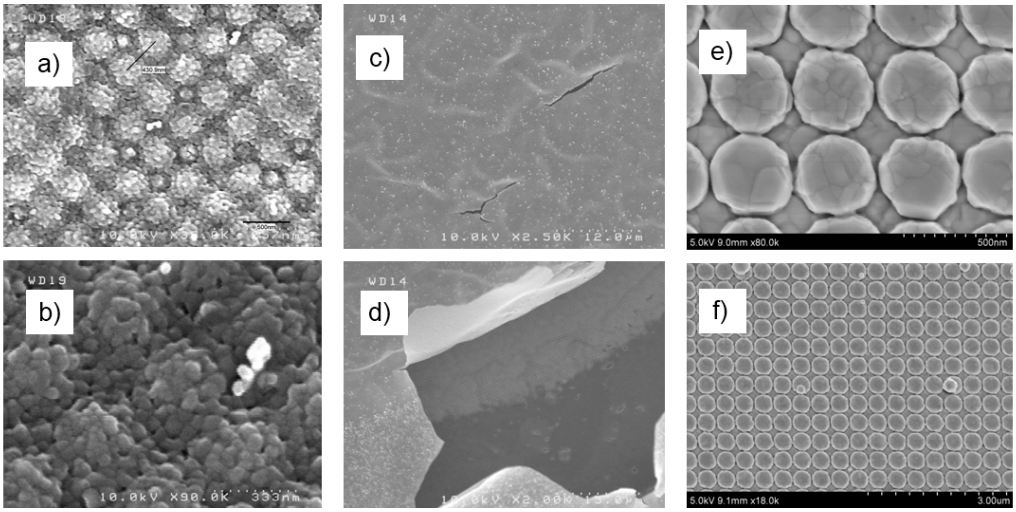

Figure 4.4: Scanning electron microscope images of damage induced to gold nanodomes by high-energy oxygen plasma treatments. (a)-(b) 2-minute treatment with plasma generator power P = 100W. (c)-(d) 10-minute treatment at P = 100W. (e)-(f) 75-second treatment at P = 50W: no apparent damage observed.

the contact angle from 34° to 23° by the amount linearly proportional to the fraction of alcohol in solution. This illustrates how multiple wetting methods may be combined in different ratios to achieve a desired contact angle under experimental conditions that may be incompatible with any one of the methods used at full strength.

4.4 Hydrophilic Monolayers of 6-Mercaptohexanol

Wetting properties of a solid are determined by its outermost molecules and functional groups. Oxygen plasma improves wetting by removing organic contaminants that are more hydrophobic than the solid material itself. A complimentary approach is to introduce new molecules on the surface that are more hydrophilic than the original material. 6-mercaptohexanol is a frequently used compound in sensing applications that involve immobilized DNA aptamers [25, 26]. It is a simple unbranched six-carbon chain, whose sulfhydryl functional group on one end allows it to form densely packed self-assembled monolayers on many metal surfaces, including silver and gold, while a hydroxyl head makes such monolayers hydrophilic.

Mercaptohexanol has multiple roles in aptamer-based sensing protocols.

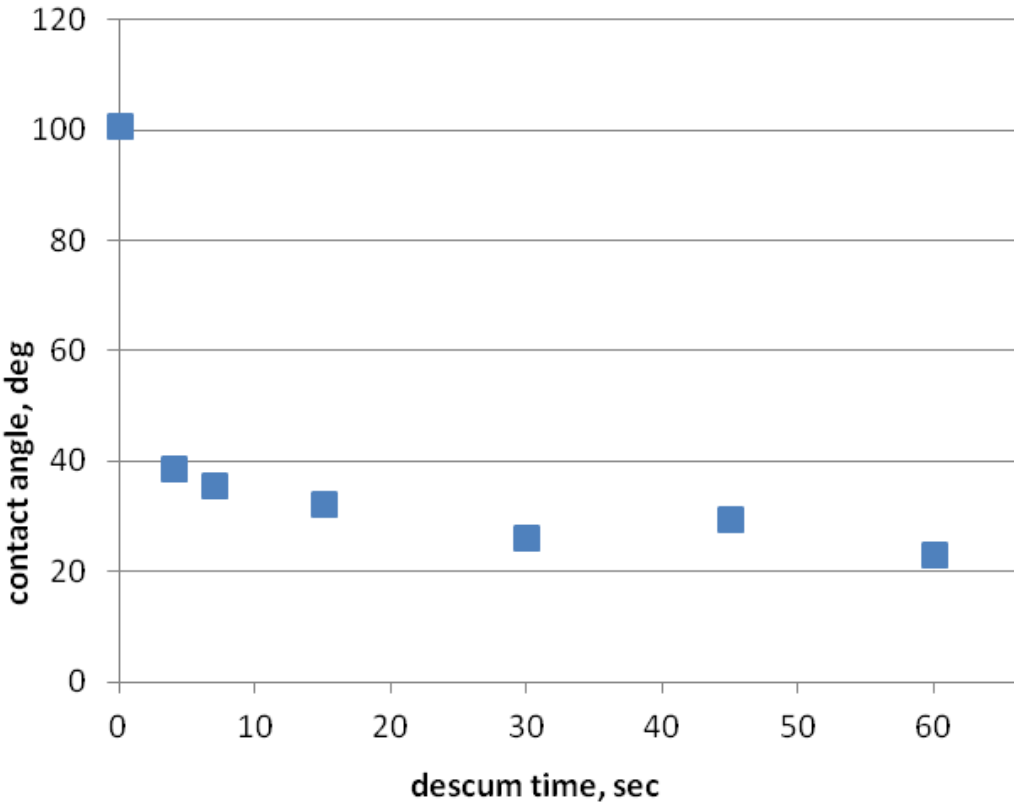

Figure 4.5: Effect of reduced-power (50W) oxygen plasma treatment on surface wetting of gold nanodomes by 6 μL 20% ethanol drops.

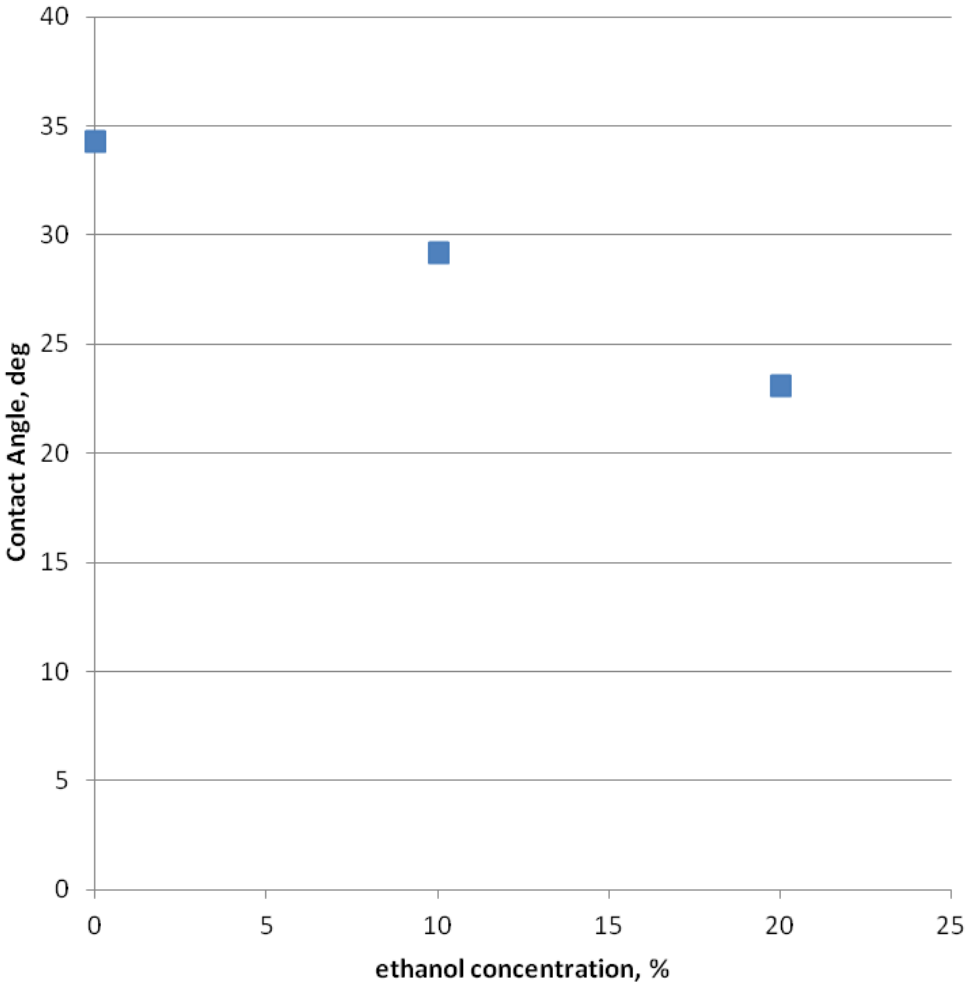

Figure 4.6: Incremental reduction of the contact angle of a 6 μL water drop on a plasma-treated nanodomes surface (t = 60 sec, P = 50 W) caused by addition of ethanol.

It passivates surfaces following sensor functionalization with DNA aptamer ligands. Smaller mercaptohexanol molecules efficiently fill spaces between larger aptamer molecules, blocking further binding of analytes or contaminants. Additionally, electrostatic repulsions between hydroxyl groups and the negatively charged aptamer backbones orient aptamer molecules away from sensor surface, improving their capturing affinity. Single-step mixed aptamer-mercaptohexanol competition monolayers have also been used to improve aptamer capture efficiency by reducing steric hindrance of capture sites via regulating aptamer monolayer density.

In the context of this work, the hydrophilic property of mercaptohexanol films is of particular interest. In order to investigate its extent, a dilution series of ethanol was spotted on coated gold surfaces. Figure 4.7 compares the resulting contact angles to those obtained in the previous ethanol series experiments. For concentrations below 30%, corresponding to the Cassie-Baxter state on untreated surfaces, the contact angle on mercaptohexanol consistently reduced by more than 50 degrees. In particular, the contact angle of neat DI water reduced from 127° to 71°. The reference measurements on coated flat gold surfaces closely agreed with those on nanodomes, confirming complete wetting of nanofeatures.

Although this approach did not produce the best reduction of contact angle, it was sufficient to induce a complete wetting of the nanodomes. It also has multiple important practical advantages. A mercaptohexanol coating step can be easily incorporated into existing sensing protocols because it is surface-bound and does not modify components of the solution. It also has a much longer lasting effect than oxygen plasma, because gold-sulfur bonds of aliphatic alkyl sulfides are thermodynamically stable at temperatures below at least 150-200 °C and are not affected by solvents [27], whereas the effect of oxygen plasma treatment diminishes in course of hours or days. Monolayers do not have a significant effect on the reduction of hot spot volumes because their thickness is too shallow. Assuming a 58° bonding angle with respect to the flat surface, the thickness of a mercaptohexanol monolayer is only 0.91 nm [28].

The significant downside of the monolayer approach is its incompatibility with sensing protocols that rely on direct analyte binding to metal surfaces, such as those for MTS-R6G and BPE Raman dyes. It also cannot be used for immobilization of ligands: even if they penetrate into hot spot regions,

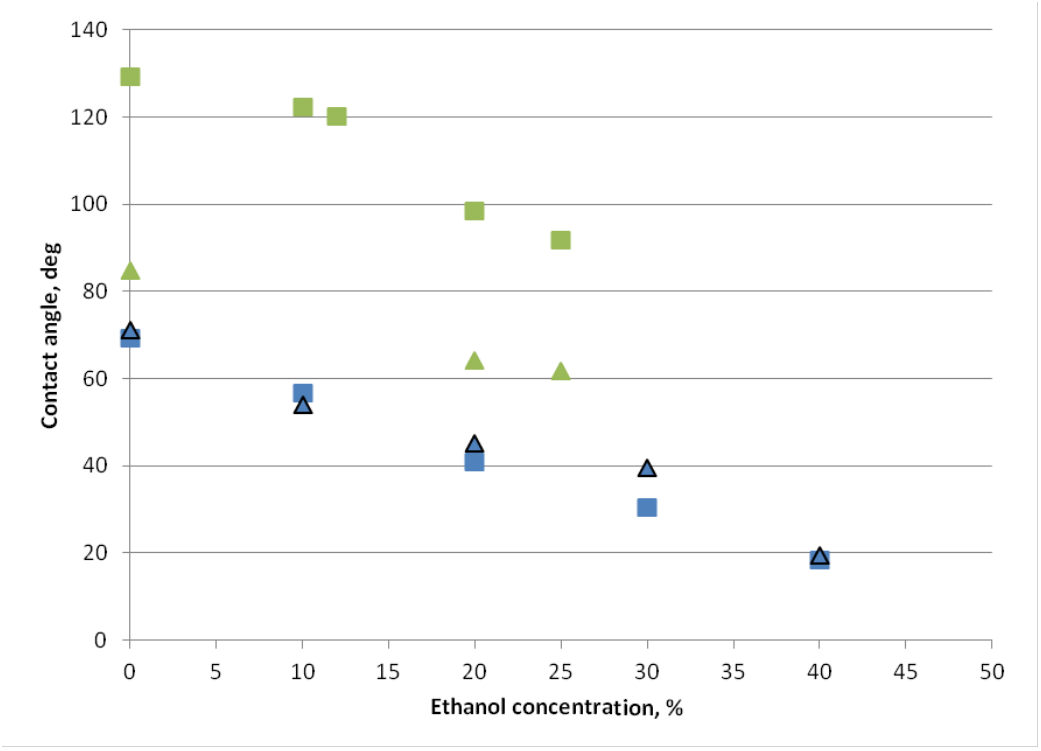

Figure 4.7: Contact angle reduction of an ethanol dilution series on flat (blue triangles) and patterned (blue squares) gold surfaces coated with 6-mercaptohexanol monolayer. Data for an analogous ethanol concentration series on uncoated flat (green triangles) and patterned (green squares) gold regions is re-plotted for clarity.

they would not be able to bind to already passivated surfaces.

There is an important distinction between ligands and analytes. The immobilization of the former is considered a part of sensor fabrication/functionalization stage, which can generally be more elaborated and rely on special tools, such as a reactive ion etcher, and special chemicals, such as surfactants. Any of the other wetting techniques discussed here is acceptable for ligand immobilization. Once done, it could be followed by a mercaptohexanol coating step, to improve future analyte permeation into the hot spots already functionalized with ligands. This simplifies sensor utilization, which should be kept as easy and straightforward for an end-user as possible. Of all the wetting methods considered here, only hydrophilic monolayers allow shifting the task of enhancing sensor hydrophilicicy onto the sensor maker.

4.5 Addition of Surfactants

Surfactants are compounds that lower the surface tension of a liquid or the interfacial tension between a liquid and a solid or another liquid. They are usually organic molecules that contain both hydrophobic and hydrophilic parts. When added to water under the right conditions, surfactant molecules aggregate along the surface, with their hydrophilic heads pointing inward and the hydrophobic tails extending outward. This alignment changes the molecular composition of the surface of water and, consequently, its wetting properties.

Addition of surfactants reduces surface tension of a liquid. Surfactants are much more efficient in modifying wetting properties of water than ethanol. Wetting is a surface property that is determined by a few outermost molecular layers of the liquid. Since ethanol is miscible with water, it uniformly distributes throughout water's volume, and only a tiny fraction of added ethanol molecules ends up on the surface. On the other hand, surfactant molecules diffuse to the surface of water and form a monolayer. Consequently, whereas 35% of ethanol is needed to reduce surface tension of water to $\sim$33 mN/m, 0.01% of either Triton X-100 or Tween-20 reduce it to nearly $\sim$31 mN/m.

Tween-20, Triton X-100 and sodium dodecyl sulfate (SDS) were the three surfactants tested in this study. The tested concentrations of 0.1 and 0.01% are the typical concentrations, at which these compounds are used. Similarly

to other experiments described in the preceding sections, the contact angles for flat and patterned regions were measured for each solution, and DI water on flat gold was used as a reference.

Figure 4.8 shows the contact angle dynamics of Tween-20 solutions of both types of surfaces. The concentration of 0.01% moderately reduced the contact angle, but insufficiently to cause a wetting state transition, as evidenced from a large separation from the curves corresponding to the two surface types. An increase in concentration resulted in a stronger hydrophilic effect, and the contact angle curve on patterned gold surfaces collapsed onto the curve for flat gold.

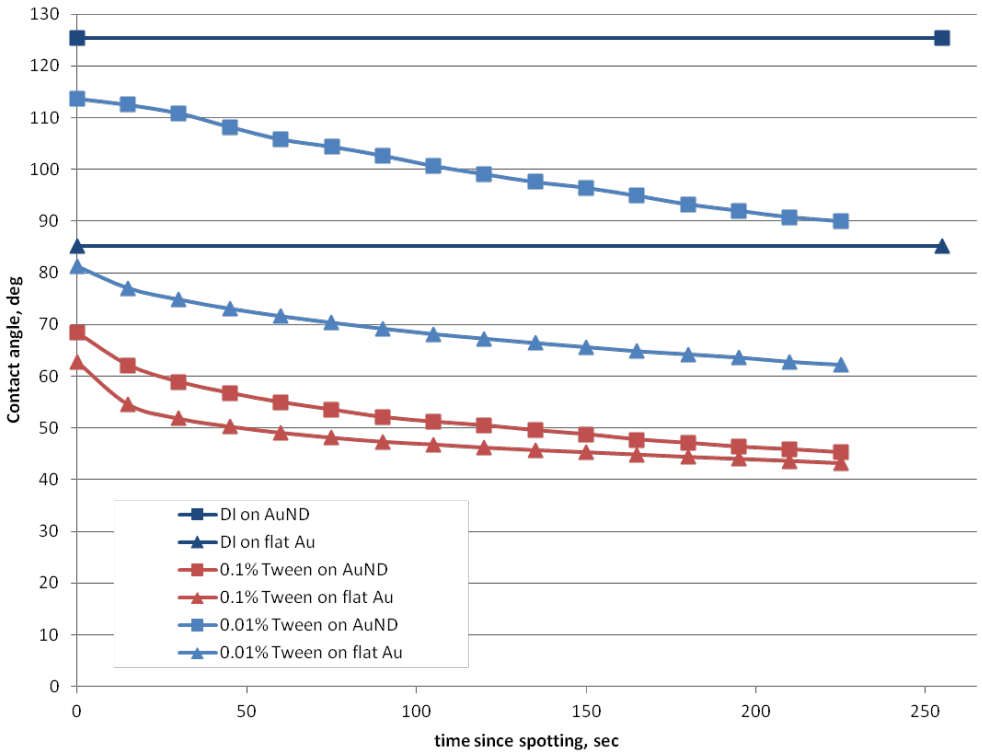

Figure 4.8: Time evolution of contact angles of 6 μL drops of 0.1% (red) and 0.01% (blue) solutions of Tween-20 on flat (triangles) and patterned (squares) gold surfaces immediately following the spotting. The dark blue lines represent the reference contact angles of pure DI water on the two types of untreated gold surfaces.

The wetting effect of Triton X-100 was more pronounced. As shown on Figure 4.9, even though the lower concentration did not result in complete wetting, either, the initial contact angle reduction was thrice that for Tween-

20. At 0.1% concentration, the contact angle became very shallow, crossing the 30° line, and very similar to that in oxygen plasma experiments.

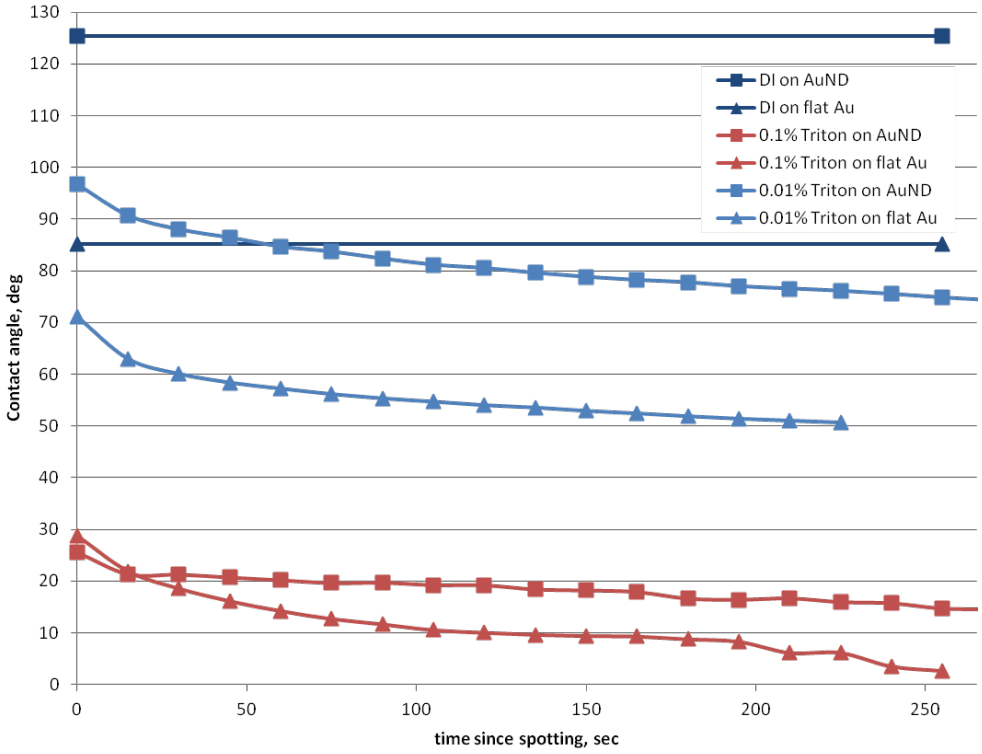

Figure 4.9: Time evolution of contact angles of 6 μL drops of 0.1% (red) and 0.01% (blue) solutions of Triton X-100 on flat (triangles) and patterned (squares) gold surfaces immediately following the spotting. The dark blue lines represent the reference contact angles of pure DI water on the two types of untreated gold surfaces.

Finally, SDS did not significantly improve surface wetting. At the highest tested concentration, it produced mediocre reduction of contact angle similar to the effect of the lower concentration of Tween-20 (see Figure 4.10).

Figure 4.11 provides a side-by-side comparison of the shallowest contact angles achieved with the three surfactants, and shows the corresponding photographs of drops taken immediately following the deposition. Both Triton X-100 and Tween-20 resulted in complete wetting, as evidenced from similar contact angle traces, with Triton X-100 being the obvious leader.

A notable difference of this experiment from those discussed previously was how slowly drops assumed an equilibrium position. In the first minutes following the deposition, drops spread slowly and gradually, complicating the

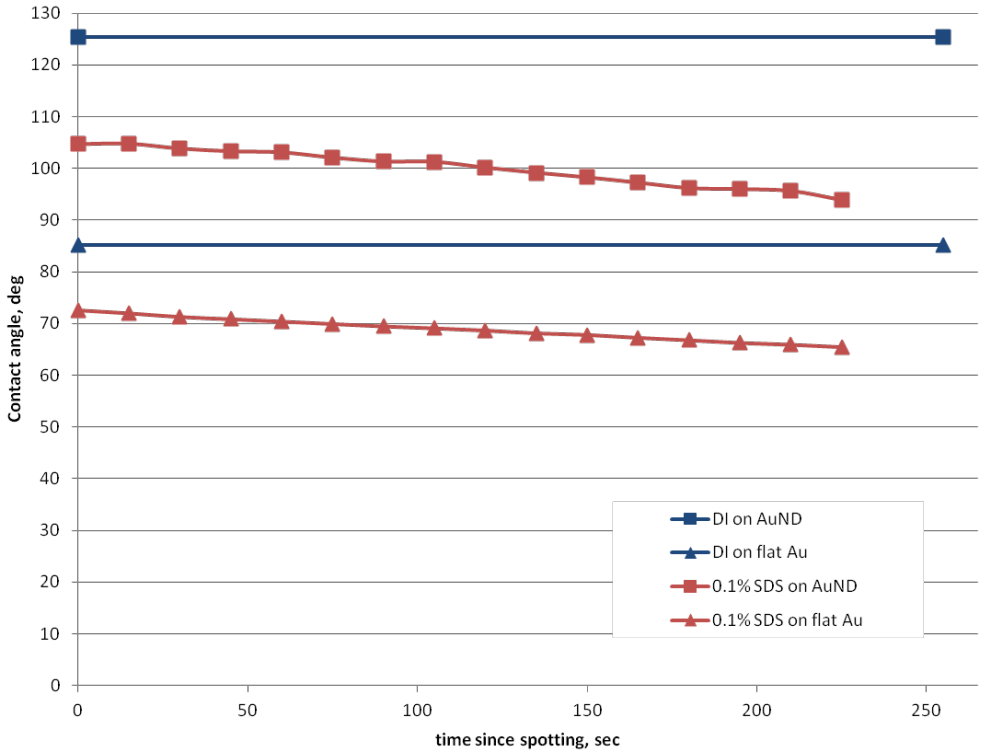

Figure 4.10: Time evolution of contact angles of 6 μL drops of 0.1% (red) solution of SDS on flat (triangles) and patterned (squares) gold surfaces immediately following the spotting. The dark blue lines represent the reference contact angles of pure DI water on the two types of untreated gold surfaces.

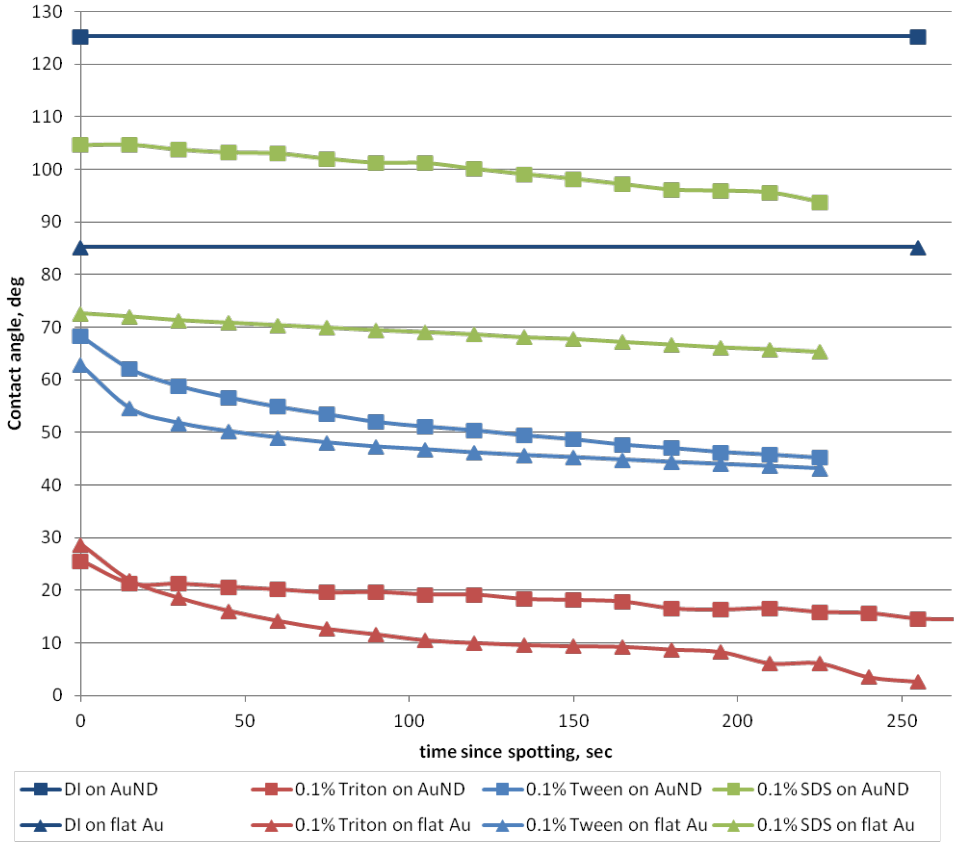

Figure 4.11: Side-by-side comparison of surface wetting improvements resulting from addition of 0.1% of SDS (green), Tween-20 (blue) or Triton X-100 (red) to pure water. Drops with volume of 6 μL were compared flat (triangles) and patterned (squares) gold surfaces.

determination of the contact angle. A possible explanation is the finite diffusion rate of the surfactants on the surface of water. The rate of advancement of the newly formed solid-liquid interface lined with surfactant molecules was limited by the depletion of the surfactant along the advancing front; it had to be replenished by diffusion from the surface of the drop exposed to air. Although the determination of exact CA values is not a goal of this work, the effect of slow spreading can be factored out, as described next.

In order to determine the true steady-state CA values, extended CA measurements were performed, and the effect of evaporation on contact angle was accounted for through the reduction of drop volume. Both the contact angle and drop volume were measured at 15 second intervals over the span of 4 minutes and are shown side-by-side on Figure 4.12. The effect of evaporation was excluded by normalizing the contact angle measurements by the corresponding volumes. The resulting plot had two distinct regions. Immediately following the drop placement, spreading significantly contributed to the reduction of the contact angle. After the first 75 seconds, any further reduction in the contact angle of 0.1% Triton X-100 was accounted for by volume reduction alone. Note that τ depends on a surfactant.

To compute the true CA value that could be compared with other approaches, for example, with the CA of DI water, the effect of spreading must be excluded. First, the time τ required for a drop of a given solution to assume an equilibrium shape on a patterned surface is determined from a volume-normalized CA plot. Next, the effect of evaporation during this time can be excluded by a linear extrapolation of the non-normalized CA at time $t = \tau$ back to the time of drop placement, $t = 0$, using the slope of the non-normalized CA at time τ:

$$CA(0) = CA(\tau) + \tau \frac{d}{dt} CA \Big|_{\tau} \tag{4.1}$$

The contact angles of water and ethanol solutions used in other experiments were not affected by extended drop spreading. For example, the CA data for a substrate treated with oxygen plasma for 60 seconds was subjected to the same analysis, as shown on Figure 4.13. In contrast to surfactants, there is no transient region corresponding to spreading. The contact angle changed by less than 1° over the course of two minutes: well within the margin of measurement error. This confirms that that the contact angles of water and

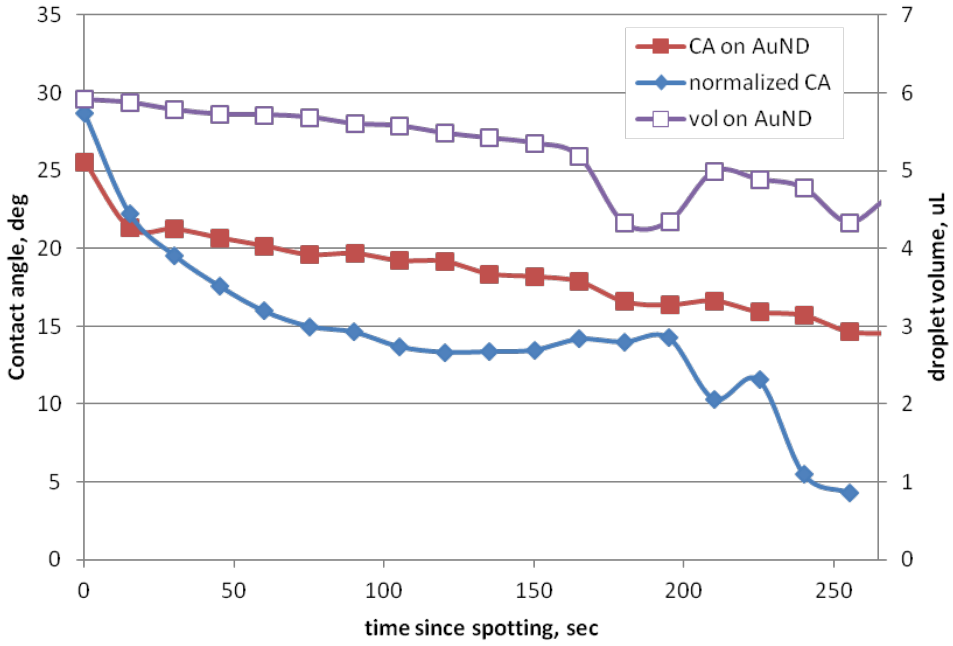

Figure 4.12: Correction for the slow spreading of solvent in the contact angle value. The apparent contact angle (red squares) is normalized by the corresponding drop volume (purple squares), producing a normalized CA plot (blue diamonds), which exhibits transient and steady-state regions.

ethanol solutions measured within the first few seconds following the drop deposition were accurate.

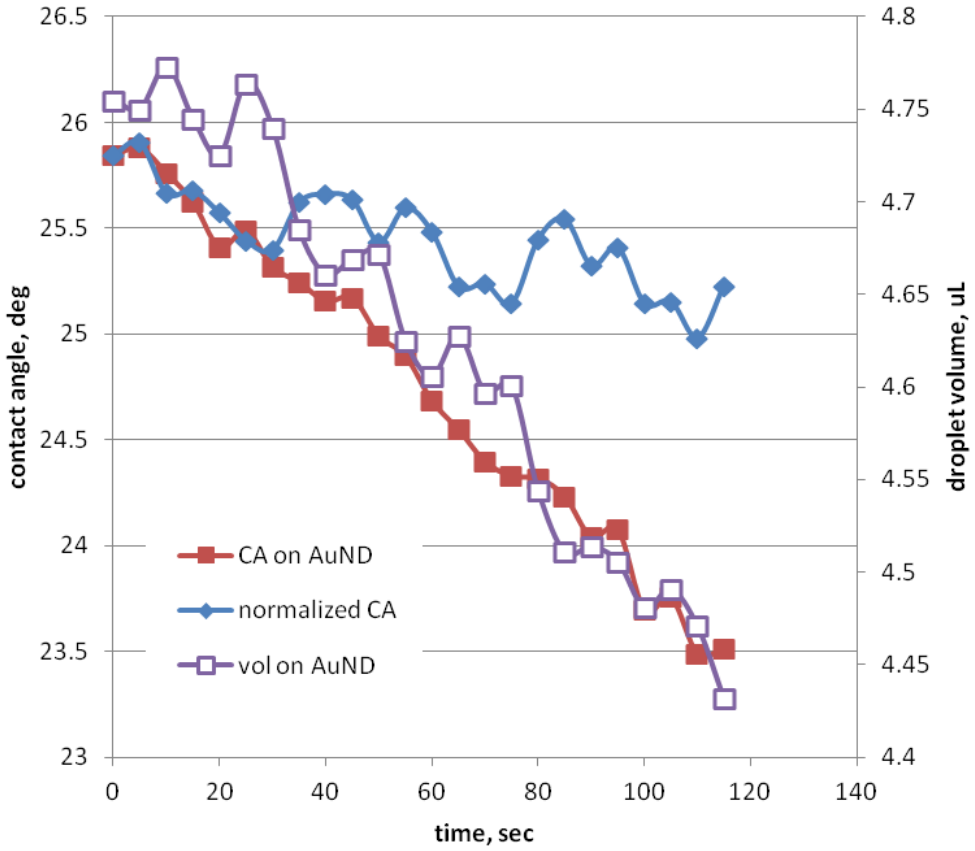

Figure 4.13: Time evolution of the contact angle (red squares) of a 6 μL 20% ethanol drop on oxygen plasma-treated nanodomes surface (t = 60 sec), and the corresponding evolution of drop volume (purple squares). The plot of normalized CA (blue diamonds) does not exhibit a transient region attributable to slow spreading of the drop.

4.6 Summary of Findings

Figure 4.14 summarizes the four techniques described previously, where better wetting corresponds to lower contact angles. The best improvement in surface wetting of gold nanodomes with pure water were achieved using any of the following methods:

- Addition of two parts of ethanol to one part water.

- A 30-second-long oxygen plasma treatment with the plasma generator power set to 50 W immediately prior to wetting the surface.
- Addition of 0.1% of Triton X-100, by volume, to water.
- Formation of a 6-mercaptohexanol monolayer on the sensor surface, combined with 20% ethanol solution.

The last method illustrates an important point: it is possible to combine multiple wetting techniques, to a different extent, to achieve a desired degree of wetting, even when individual techniques either do not have the desired strength or are incompatible with the rest of the experimental conditions.

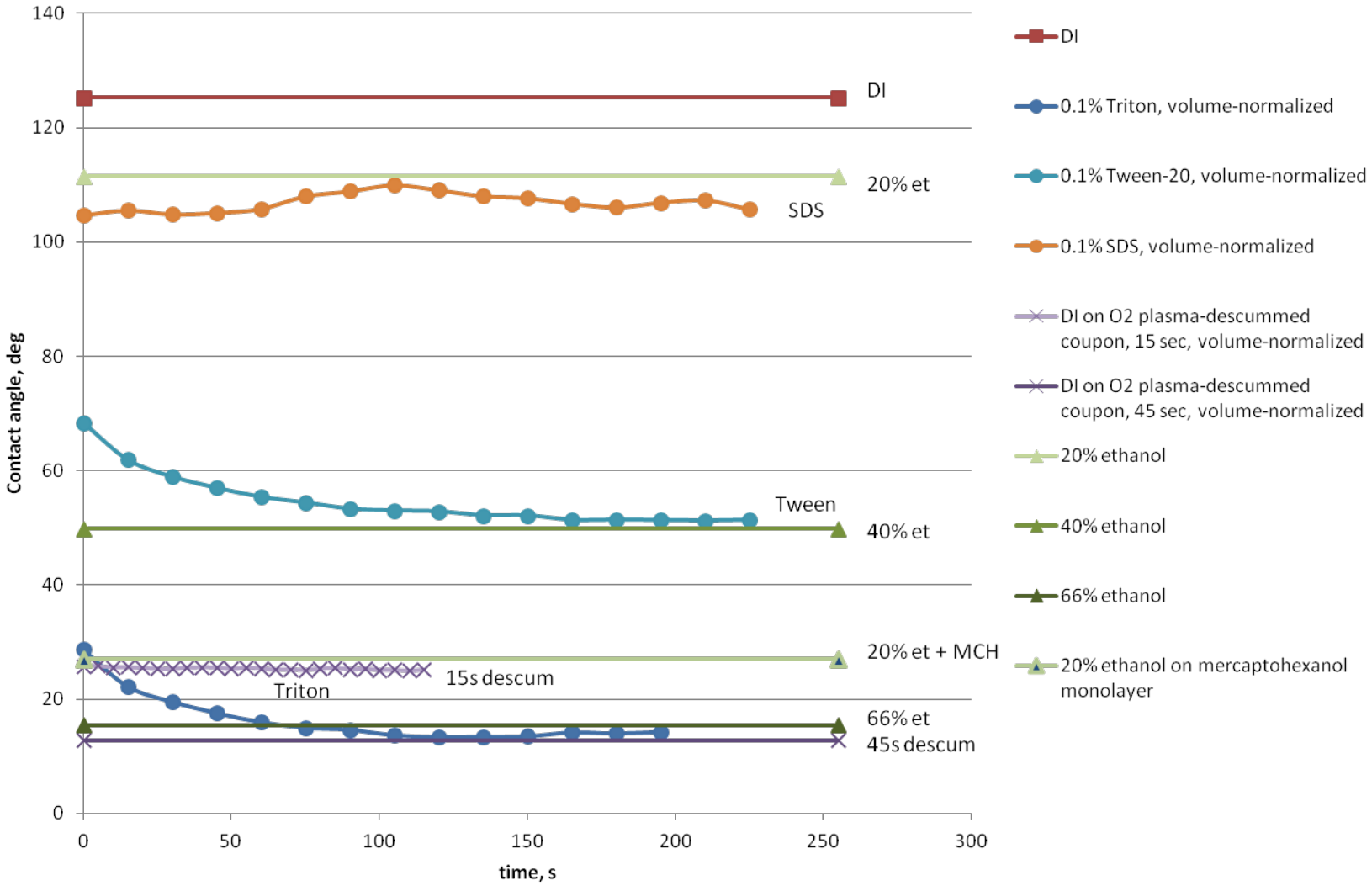

Figure 4.14: Relative effectiveness of the four wetting techniques discussed in this chapter in inducing a wetting state transition on nanodomes SERS sensors. A transition takes place near the CA = 70° mark.

CHAPTER 5

DEMONSTRATION OF IMPROVED WETTING AND FUTURE DIRECTIONS

Application of surface wetting techniques discussed in Chapter 4 allowed us to detect, for the first time, aptamer-like molecules on gold nanodome substrates using label-free surface-enhanced Raman spectroscopy. Figure 5.1 shows a SERS spectrum of thiolated single-stranded homooligoadenosine 26-mers adsorbed from 30 μL of 1 μM aqueous solution incubated directly on the sensor coupon, as well as the spectrum of background noise of the same sensor area measured immediately before the functionalization. The spectra were obtained using a $\lambda = 785$ nm excitation laser focused on the nanodomes substrate with a 20x objective, with a numerical aperture of 0.4. The total power delivered to the sample plane was 1.1 mW, and the integration time was 20 seconds. Complete wetting of nanodomes was achieved by subjecting the substrate to 30 seconds of 50 W O_2 plasma. The solvent was enhanced with 0.1% Triton X-100.

The two characteristic Raman modes of adenosine previously reported in literature [29] are located at 731 and 1320 cm^{-1}. Figure 5.2 focuses on the spectral regions of interest, after performing background subtraction, Savitsky-Golay noise filtering and rescaling. Both characteristic adenosine peaks are found sufficiently close to the reference values, at 737 and 1339 cm^{-1}, and their intensities are well above the noise floor defined as 3 times the standard deviation of noise.

A newfound ability to detect short immobilized oligonucleotides is a critical milestone in a larger scheme to transform SERS nanodomes substrates into a universal sensing platform that utilizes DNA aptamers to detect a wide variety of disease biomarkers. The success of the investigation into the wetting properties of SERS nanodomes substrates was critical, because biomarker experiments are conducted in aqueous solutions.

The results presented in this thesis will pave the way toward the next milestones, which consist of demonstrating reliable detection of other simple

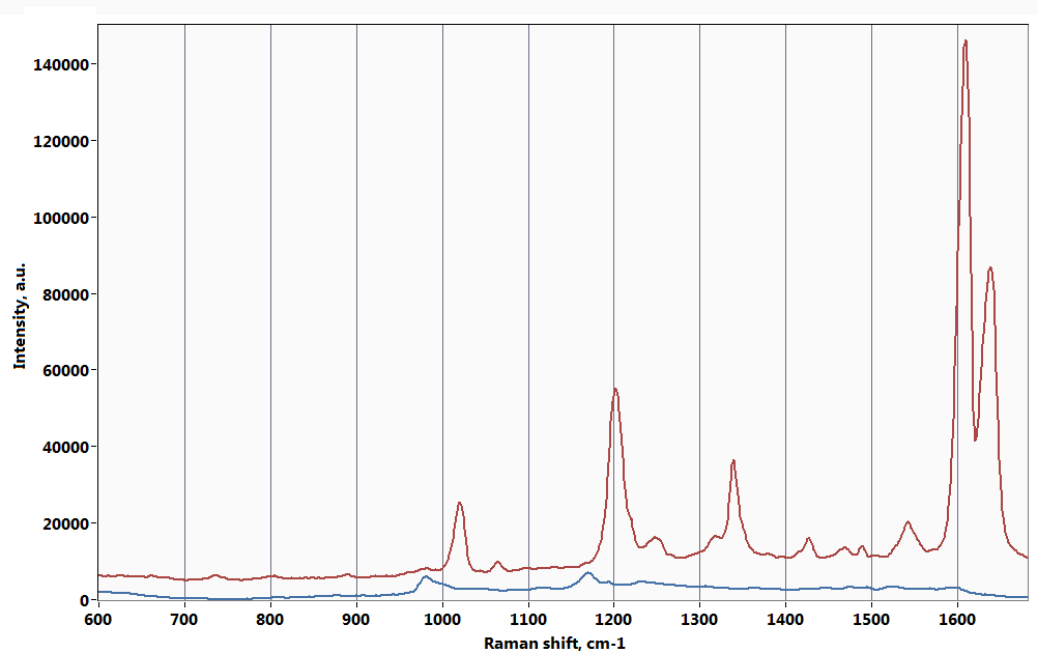

Figure 5.1: SERS spectrum of thiolated single-stranded homooligoadenosine 26-mers (red) adsorbed from 1 μM solution and a corresponding background spectrum (blue) acquired immediately before the immobilization. Surface wetting is enhanced by 30 seconds of oxygen plasma at 50 W and 0.1% of Triton X-100.

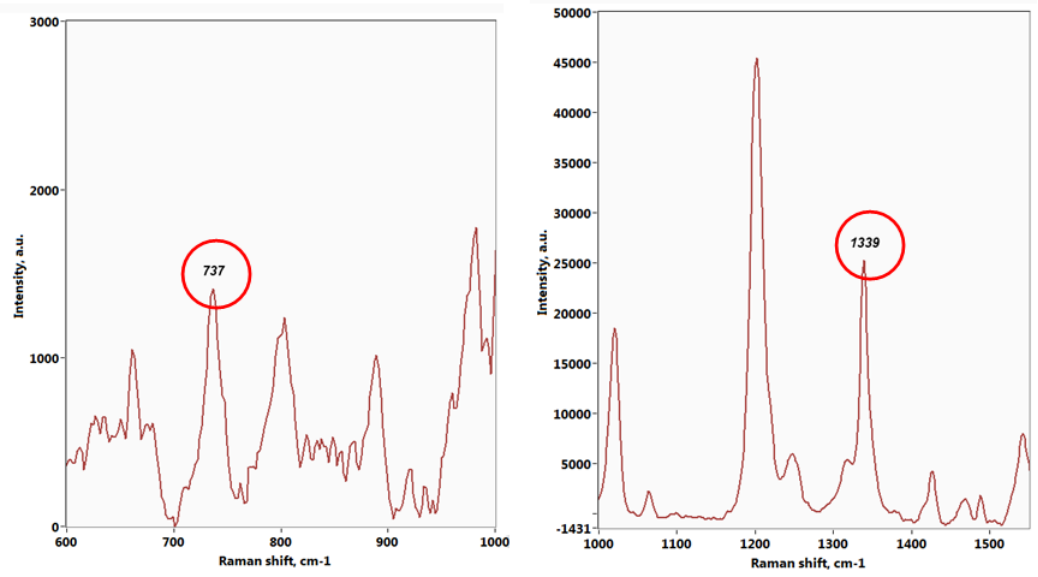

Figure 5.2: The SERS spectrum of 1 μM homooligoadenosine after noise reduction and background removal. The two highlighted peaks located at 737 and 1339 cm^{-1} are the characteristic SERS peaks of oligoadenosine.

homooligonucleotides and studying how composition, conformation and hybridization state of oligonucleotides manifest themselves spectrally. Once the relationships between physical and spectral properties are established, they will be used to help recognize binding events between real DNA aptamers and their targets. For instance, if a double-stranded DNA aptamer was designed to dehybridize when capturing its target, then the presence of analyte could be discovered from the changes in spectral properties of the aptamers, which is especially advantageous for analytes that do not have strong SERS signatures. The ultimate goal of this project is to parallelize the technique for single analyte detection, to develop a multiplexed biomarker screening platform capable of concurrent diagnosis of multiple complex diseases.

REFERENCES

[1] A. Marmur, "Wetting on hydrophobic rough surfaces: To be heterogeneous or not to be?" *Langmuir*, vol. 19, no. 20, pp. 8343–8348, Aug. 2003.

[2] J. Homola, S. S. Yee, and G. Gauglitz, "Surface plasmon resonance sensors: Review," *Sensors and Actuators B: Chemical*, vol. 54, no. 1-2, pp. 3–15, 1999.

[3] R. C. Jorgenson and S. S. Yee, "A fiber-optic chemical sensor based on surface plasmon resonance," *Sensors and Actuators B: Chemical*, vol. 12, no. 3, pp. 213–220, 1993.

[4] L. M. Zhang and D. Uttamchandani, "Optical chemical sensing employing surface plasmon resonance," *Electronics Letters*, vol. 24, no. 23, pp. 1469–1470, 1988.

[5] C. Nylander, B. Liedberg, and T. Lind, "Gas detection by means of surface plasmon resonance," *Sensors and Actuators*, vol. 3, pp. 79–88, 1983.

[6] B. Liedberg, C. Nylander, and I. Lunstrom, "Surface plasmon resonance for gas detection and biosensing," *Sensors and Actuators*, vol. 4, pp. 299–304, 1983.

[7] B. Liedberg, I. Lundstrom, and E. Stenberg, "Principles of biosensing with an extended coupling matrix and surface plasmon resonance," *Sensors and Actuators B: Chemical*, vol. 11, no. 1, pp. 63–72, 1993.

[8] K. Matsubara, S. Kawata, and S. Minami, "Optical chemical sensor based on surface plasmon measurement," *Applied Optics*, vol. 27, no. 6, pp. 1160–1163, 1988.

[9] D. R. Mernagh, P. Janscak, K. Firman, and G. G. Kneale, "Protein-protein and protein-DNA interactions in the type I restriction endonuclease R.EcoR124I," *Biological Chemistry*, vol. 379, no. 4, pp. 497–504, 1998.

[10] V. Regnault, J. Arvieux, L. Vallar, and T. Lecompte, "Immunopurification of human β_2-glycoprotein I with a monoclonal antibody selected for its binding kinetics using a surface plasmon resonance biosensor," *Journal of Immunological Methods*, vol. 211, no. 1-2, pp. 191–197, 1998.

[11] J. Deka, J. Kuhlmann, and O. Muller, "A domain within the tumor suppressor protein APC shows very similar biochemical properties as the microtubule-associated protein tau," *European Journal of Biochemistry*, vol. 253, no. 3, pp. 591–597, 1998.

[12] C. F. Boliren and D. R. Huffman, *Absorption and Scattering of Light by Small Particles*. Wiley & Sons, 1983.

[13] M. Fleischmann, P. J. Hendra, and A. J. McQuillan, "Raman spectra of pyridine adsorbed at a silver electrode," *Chemical Physics Letters*, vol. 26, no. 2, pp. 163–166, 1974.

[14] D. L. Jeanmaire and R. P. Van Duyne, "Surface Raman spectroelectrochemistry: Part I. Heterocyclic, aromatic, and aliphatic amines adsorbed on the anodized silver electrode," *Journal of Electroanalytical Chemistry and Interfacial Electrochemistry*, vol. 84, no. 1, pp. 1–20, 1977.

[15] A. Otto, "The 'chemical'(electronic) contribution to surface-enhanced Raman scattering," *Journal of Raman Spectroscopy*, vol. 36, no. 6-7, pp. 497–509, 2005.

[16] E. Ru, E. Blackie, M. Meyer, and P. Etchegoin, "Surface enhanced Raman scattering enhancement factors: A comprehensive study," *Journal of Physical Chemistry C*, vol. 111, no. 37, pp. 13 794–13 803, Sep. 2007.

[17] Y. Chu, M. G. Banaee, and K. B. Crozier, "Double-resonance plasmon substrates for surface-enhanced Raman scattering with enhancement at excitation and Stokes frequencies," *ACS Nano*, vol. 4, no. 5, pp. 2804–2810, 2010.

[18] H. Ko, S. Singamaneni, and V. V. Tsukruk, "Nanostructured surfaces and assemblies as SERS media," *Small*, vol. 4, pp. 1576–1599, Oct. 2008.

[19] P. Stiles, J. Dieringer, N. Shah, and R. Van Duyne, "Surface-enhanced Raman spectroscopy," *Annual Review of Analytical Chemistry*, vol. 1, pp. 601–626, 2008.

[20] C. J. Choi, Z. Xu, H. Y. Wu, G. L. Liu, and B. T. Cunningham, "Surface-enhanced Raman nanodomes," *Nanotechnology*, vol. 21, p. 415301, 2010.

[21] A. B. D. Cassie and S. Baxter, "Wettability of porous surfaces," *Transactions of the Faraday Society*, vol. 40, pp. 546–551, 1944.

[22] R. N. Wenzel, "Resistance of solid surfaces to wetting by water," *Industrial & Engineering Chemistry*, vol. 28, no. 8, pp. 988–994, 1936.

[23] C. Ishino and K. Okumura, "Wetting transitions on textured hydrophilic surfaces," *The European Physical Journal E*, vol. 25, no. 4, pp. 415–424, Apr. 2008.

[24] G. Vazquez, E. Alvarez, and J. M. Navaza, "Surface tension of alcohol water + water from 20 to 50° C," *Journal of Chemical & Engineering Data*, vol. 40, no. 3, pp. 611–614, May 1995.

[25] T. M. Herne and M. J. Tarlov, "Characterization of DNA probes immobilized on gold surfaces," *Journal of the American Chemical Society*, vol. 119, no. 38, pp. 8916–8920, 1997.

[26] D. P. Wernette, C. Mead, P. W. Bohn, and Y. Lu, "Surface immobilization of catalytic beacons based on ratiometric fluorescent DNAzyme sensors: A systematic study," *Langmuir*, vol. 23, pp. 9513–9521, Aug. 2007.

[27] R. G. Nuzzo, F. A. Fusco, and D. L. Allara, "Spontaneously organized molecular assemblies. 3. Preparation and properties of solution adsorbed monolayers of organic disulfides on gold surfaces," *Journal of the American Chemical Society*, vol. 109, no. 8, pp. 2358–2368, Apr. 1987.

[28] T. Huang, P. D. Nallathamby, and X.-H. N. Xu, "Photostable single-molecule nanoparticle optical biosensors for real-time sensing of single cytokine molecules and their binding reactions," *Journal of the American Chemical Society*, vol. 130, no. 50, pp. 17 095–17 105, Nov. 2008.

[29] M. Green, F.-M. Liu, L. Cohen, P. Kollensperger, and T. Cass, "SERS platforms for high density DNA arrays," *Faraday Discussions*, vol. 132, p. 269, 2006.